THE ASTROPHYSICAL JOURNAL, 415:397–414, 1993 September 20

THEORETICAL MODELING OF THE INFRARED FLUORESCENCE FROM INTERSTELLAR POLYCYCLIC AROMATIC HYDROCARBONS

W. A. SCHUTTE,[1] A. G. G. M. TIELENS, AND L. J. ALLAMANDOLA
Space Science Division, NASA/Ames Research Center, MS:245-6, Moffett Field, CA 94035-1000
Received 1992 February 10; accepted 1993 March 29

ABSTRACT

We have modeled the family of interstellar IR emission bands at 3.3, 6.2, 7.7, 8.6, 11.3, and 12.7 μm by calculating the fluorescence from a size distribution of interstellar polycyclic aromatic hydrocarbons (PAHs) embedded in the radiation field of a hot star. It is found that the various emission bands are dominated by distinctly different PAHs, from molecules with much less than $\sim$80 C atoms for the 3.3 μm feature, to molecules with 10^2–10^5 C atoms for the emission in the *IRAS* 12 and 25 μm bands. We quantitatively describe the influence on the emergent spectrum of various PAH properties such as the molecular structure, the amount of dehydrogenation, the intrinsic strength of the IR active modes, and the size distribution. Comparing our model results to the emission spectrum from the Orion Bar region, we conclude that interstellar PAHs are likely fully, or almost fully, hydrogenated. Moreover, it is found that the intrinsic strengths of the 6.2 and 7.7 μm C—C stretching modes, and the 8.6 μm C—H in-plane bending mode are 2–6 times larger than measured for neutral PAHs in the laboratory. This difference is tentatively ascribed to interstellar PAHs being ionized, or, alternatively, to their being highly asymmetric. It is furthermore concluded that the earlier assignment of the 3.4 μm subfeature to the hot band of the aromatic C—H stretching mode is only marginally consistent with the available observational data. In some cases an additional component appears to be required to account for its intensity. The hot band may be responsible for a weaker shoulder in some cases. An assignment to the C—H stretching feature from "superhydrogenated" PAHs, i.e., PAHs with extra H atoms attached to the peripheral carbon atoms, is considered as the additional contributor. Finally, it is pointed out how future high-quality observations of the emission from interstellar PAHs covering a large wavelength range, together with modeling of the type presented in the paper, could be used to study a number of important questions, such the preferred molecular structures of interstellar PAHs and their evolution in the interstellar medium.

Subject headings: infrared: interstellar: lines — ISM: molecules — line: identifications — molecular processes

1. INTRODUCTION

A distinctive set of IR emission features at 3.3, 6.2, 7.7, 8.7, 11.3, and 12.7 μm originate in the vicinity of a large number of hot stellar sources including H II regions, reflection nebulae, planetary nebulae, proto–planetary nebulae, and galactic nuclei (e.g., Russell, Soifer, & Merrill 1977a, Russell, Soifer, & Willner 1977b; Cohen, Tielens, & Allamandola 1985; Cohen et al. 1986, 1989; de Muizon et al. 1986; Phillips, Aitken, & Roche 1984; Roche & Aitken 1985; Roche, Aitken, & Smith 1989; Jourdain de Muizon, d'Hendecourt, & Geballe 1990a; Buss et al. 1990). These features have been assigned to emission from interstellar polycyclic aromatic hydrocarbon (PAH) molecules, which become vibrationally excited upon absorption of a UV photon and subsequently lose their excess energy through IR fluorescence (Duley & Williams 1981; Sellgren 1984; Léger & Puget 1984; Allamandola, Tielens, & Barker 1985). Average PAH sizes based on the observed intensity ratio of the 3.3 μm C—H stretching feature and the 11.3 μm C—H out-of-plane bending feature have been variably estimated to lie between 20 and 100 carbon atoms (Leger & Puget 1984; Allamandola et al. 1985; Allamandola, Tielens, & Barker 1989, hereafter ATB; Cohen et al. 1986; Jourdain de Muizon et al. 1990a; Léger & d'Hendecourt 1987). However, larger PAHs or PAH clusters ($\sim$500 C atoms) are thought to be responsible for the broad emission plateaus underlying the narrow 6.2 and 7.7 μm features (Cohen et al. 1986; Bregman et al. 1989). Likewise, the widespread 60 μm cirrus emission in the Galaxy is at least partially emitted by even larger structures (up to 50 Å). Thus, the observations imply that the grain size distribution of interstellar carbon grains extends well into the molecular domain (Tielens 1989).

Although the general identification with molecular-sized PAHs is supported by both the wavelength of the features and their relative strengths, many properties of these molecules remain unclear. For example, based on observational or theoretical grounds, it has been alternatively suggested that interstellar PAHs are either severely dehydrogenated (by $\sim$90%; Léger & d'Hendecourt 1987 and Jourdain de Muizon et al. 1990a), or that dehydrogenation is negligible (Tielens et al. 1987; ATB). Likewise, the detailed spectral structure in the 3–4 μm region has been alternatively interpreted as indicating the presence of aliphatic sidegroups on the aromatic carbon skeleton (Duley & Williams 1981; de Muizon et al. 1986) or as originating from hot bands, and overtone and combination bands of the PAH fundamentals (Barker, Allamandola, & Tielens 1987; Geballe et al. 1989).

Past modeling of the IR emission spectrum has often approached the problem from the "classic grain" side. That is, the properties of the small grains/large molecules were based upon an extrapolation of those of large ($\sim$100 Å) graphitic grains (Draine & Anderson 1985; Dwek 1986). However, large graphitic grains form a poor template for the properties of

[1] Current address: Laboratory Astrophysics, Huygens Laboratory, Leiden University, The Netherlands.

small grains/large molecules (Léger & Puget 1984; Allamandola et al. 1985; ATB). More realistic models of the emission from interstellar PAHs used laboratory measured frequencies for the molecular vibrations and cross sections of the IR bands (Puget, Leger, & Boulanger 1985; Allamandola et al. 1985, 1989; Puget & Leger 1989; Désert, Boulanger, & Puget 1990). Some of these previous models attempted to incorporate the PAHs in an overall grain model which would simultaneously fit the interstellar emission and absorption curve. However, there are many uncertainties in such an approach since the contribution from larger grains (i.e., $a > 50$ Å) to the general extinction overwhelms that of the PAHs. Indeed, the carrier of the IR emission features is known to be responsible for only 5% of the UV and or visible extinction in many (not all) of the emission objects (Allamandola et al. 1985). Moreover, many other materials are thought to be present in interstellar dust, including silicates, SiC, diamonds, organic grain mantles, HAC, etc. For this reason we will concentrate on the PAH related details for the IR emission spectrum.

It is the purpose of this paper to develop a more comprehensive model of the family of interstellar IR emission features by calculating the emission spectrum from a continuous size distribution of PAHs embedded in the radiation field of a hot star. This will enable us to study quantitatively how parameters such as the molecular structure of the PAHs, their degree of hydrogenation, the intrinsic strengths of the various IR modes, and the PAH size distribution influence the observed spectrum. By comparing these results to observations, a better understanding of the properties of interstellar PAHs may be obtained and future laboratory studies can be guided.

The paper is laid out as follows. In § 2 our method of calculating the fluorescence of a vibrationally excited PAH molecule is described. In § 3 the various free parameters involved in modeling the emission by interstellar PAHs are discussed. In § 4 calculated spectra are presented and the influence of the free parameters are investigated. Section 5 compares the model results to observations of the IR emission bands, leading to a number of conclusions on the properties of interstellar PAHs. These results are summarized in § 6.

2. IR FLUORESCENCE MODELS

The emission intensity associated with an IR active fundamental vibrational transition, i, from level v to level $(v-1)$, in a molecule with a total internal vibrational energy E (i.e., the energy deposited by the absorption of a photon) is given by (ATB)

$$I(E, i, v) = h\nu_i v A_i^{1,0} \frac{\rho_r(E - vh\nu_i)}{\rho(E)}, \quad (1)$$

where h is the Planck constant, v is the vibrational quantum number, ν_i is the frequency of the emitting mode, $A_i^{1,0}$ is the Einstein coefficient of the $1 \rightarrow 0$ transition, $\rho(E)$ is the density of vibrational states at total internal energy E, and $\rho_r(E - vh\nu_i)$ is the density of vibrational states for all modes except the emitting mode at a vibrational energy equal to E minus the amount of energy in the emitting mode.

For nearly harmonic oscillators, the emission from the $\Delta v = 1$ transitions originating from various levels (quanta) of a particular vibrational mode are close in frequency and blend to a single emission feature with intensity:

$$I(E, i) = \sum_{v=1}^{v_{max}} I(E, i, v). \quad (2)$$

v_{max} is constrained by the finite bonding energy of the vibrational mode and the total energy available. At the vibrational energies relevant to the modeling of the emission from interstellar PAHs ($E < 100{,}000$ cm^{-1}), $I(E, i, v)$ decreases rapidly with increasing v, and no significant error is introduced when assuming that $v_{max} = \infty$.

If the frequencies of all modes of a molecule are known, equation (1) can be calculated in an exact manner using an appropriate numerical algorithm (Stein & Rabinovitch 1973). Unfortunately, for interstellar PAHs, all vibrational frequencies are not known. Moreover, the calculations involved in this approach are quite extensive, especially for large molecules or clusters of molecules containing up to 10^3 atoms which must be included to completely model the interstellar IR emission band family (§ 4). It is therefore desirable to find an approximation for equation (1) which can be applied over a very broad size range. Here we will examine two simple approximations, i.e., the thermal and the Whitten & Rabinovitch approximation, and compare them to the exact evaluation of equation (1).

The emission from vibrationally excited PAHs has been calculated using the thermal approximation (Leger & Puget 1984; Leger et al. 1989a). This model uses the Boltzmann equation to describe the excitation of the molecule. The emitted intensity is then given by

$$I[T(E), i, v] = h\nu_i v A_i^{1,0} \exp(-vh\nu_i/kT)[1 - \exp(-h\nu_i/kT)], \quad (3)$$

where T is the vibrational excitation temperature of the molecule and k is the Boltzmann constant. Summation of equation (3) from $v = 1$ to ∞ gives the familiar result

$$I[T(E), i] = h\nu_i A_i^{1,0}[\exp(h\nu_i/kT) - 1]^{-1}. \quad (4)$$

In the framework of this approximation, the total vibrational energy E and the temperature T are related through the heat capacity of the molecule, and this relation is given by

$$E(T) = \sum_{j=1}^{s} h\nu_j[\exp(h\nu_j/kT) - 1]^{-1}, \quad (5)$$

with s the number of vibrational modes in the molecule (equal to 3 times the number of atoms minus 6 for nonlinear polyatomics). The thermal model assumes that the emission from a molecule containing vibrational energy E can be approximated by the average emission of an oscillator connected to a thermal bath with temperature T. Such a canonical description is reasonably accurate if *the average energy of the mode under consideration is small compared to the total energy in the thermal bath* (Léger et al. 1989a; ATB; Barker & Cherchneff 1989; d'Hendecourt et al. 1989). However, the vibrational energy of a given mode will fluctuate around the average. Since the emitted intensity in a mode increases steeply with internal energy, equation (4) will, in general, overestimate the true emitted intensity.

Figure 1 shows the ratio of the emitted intensity calculated by the exact model and the thermal model for two modes, the C—H stretching mode at 3030 cm^{-1} (3.3 μm) and a mode at 835 cm^{-1} (12.0 μm), for three PAHs, pyrene ($C_{16}H_{10}$) and $C_{96}H_{24}$ and $C_{600}H_{60}$ (two members of "series 1" of condensed PAH molecules; see Stein & Brown 1986 and Tielens et al. 1987). The 835 cm^{-1} mode corresponds to the coupled out-of-plane bending mode of two adjacent H atoms (ATB). For the frequencies of the C—H and C—C modes of $C_{96}H_{24}$ and $C_{600}H_{60}$, we adopted the C—H and C—C frequencies of

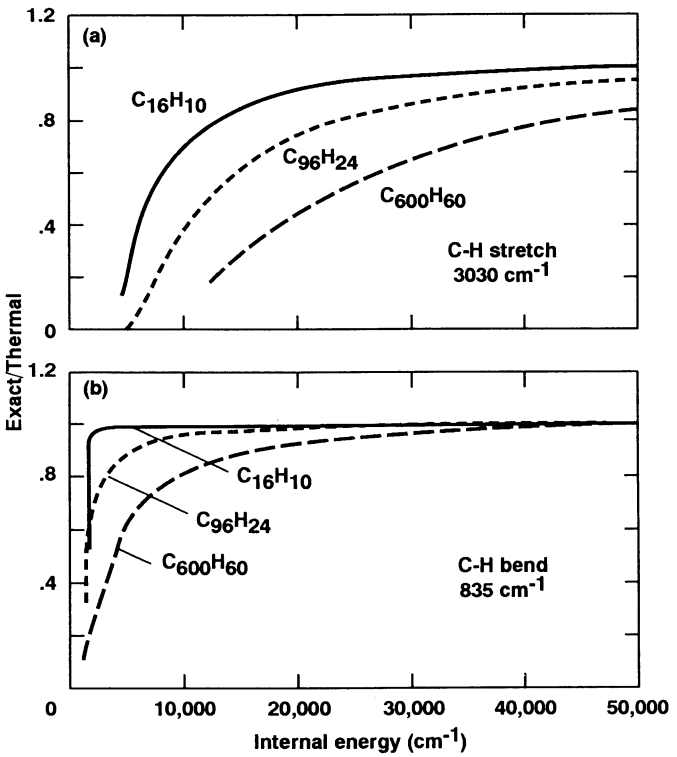

FIG. 1.—The ratio of the emitted intensity calculated by the exact method to the intensity obtained by the thermal approximation for the (*a*) 3030 cm^{-1} C—H stretching mode and the (*b*) 835 cm^{-1} C—H out-of-plane bending mode of two adjacent C—H groups, as a function of the vibrational energy of the molecule. Curves are plotted for pyrene ($C_{16}H_{10}$), $C_{96}H_{24}$, and $C_{600}H_{60}$.

pyrene (see also § 3.2.2 below). Figure 1 shows, as has been previously pointed out, that the accuracy of the thermal approximation improves with increasing energy, with decreasing frequency of the mode, and with decreasing size of the molecule (for a more detailed discussion on the dependence of the thermal approximation on these parameters we refer to ATB; d'Hendecourt et al. 1989; Léger, d'Hendecourt, & Défourneau 1989b). Generally the thermal model provides a good approximation to the emission as long as the vibrational energy of the emitting mode is less than $\sim 10\%$ of the total vibrational energy in the molecule.

Alternatively, it has been proposed to calculate equation (1) using the Whitten & Rabinovitch (WR) approximation of the density of states $\rho(E)$ (ATB). This approximation is given by (Whitten & Rabinovitch 1963):

$$\rho(E) = \left[(E + aE_0)^{s-1} \Big/ (s-1)! \prod_{j=1}^{s} h\nu_j \right] \left(1 + E_0 \frac{da}{dE} \right), \quad (6)$$

where E_0 is the zero-point energy of the molecule:

$$E_0 = 0.5 \sum_{j=1}^{s} h\nu_j \quad (7)$$

and a is given by

$$a(E) = 1 - \beta\omega(E/E_0), \quad (8)$$

where

$$\beta = \frac{(s-1)\langle \nu^2 \rangle}{s\langle \nu \rangle^2}. \quad (9)$$

ω is given as a function of E/E_0 by Whitten & Rabinovitch. Note that to obtain the reduced density of states ρ_r, the emitting ith mode should be omitted when using equations (6), (7), and (9).

Figure 2 shows the ratio of the emitted intensity given by the exact model to the intensity given by the WR approximation for the same molecules and vibrational modes that were used to compare the exact and the thermal model (Fig. 1). As with the thermal model, the precision of the WR approximation improves with increasing energy, decreasing frequency of the mode and with decreasing size of the molecule.

Comparing Figures 1 and 2, it can be seen that, although the WR approximation is about as good as the thermal model in calculating the emission of pyrene ($C_{16}H_{10}$), it deteriorates much faster with increasing molecular size. As pointed out by Whitten & Rabinovitch, the internal vibrational energy below which the WR approximation starts to deviate from the exact treatment is roughly proportional to the zero point energy of the molecule (eq. [7]; i.e., roughly proportional to the molecular size). In contrast, the energy below which the thermal approximation starts to deviate increases in a manner significantly less than proportional to the molecular size (Fig. 1). For this reason the WR approximation is considerably less accurate than the thermal approximation when calculating the IR fluorescence from large PAHs.

Since the thermal approximation is preferred over the Whitten & Rabinovitch approximation for modeling of the interstellar IR emission bands, the rest of the discussion will focus on quantifying its accuracy. As Figure 1 illustrates, for larger molecules, the relative difference between the thermal and exact models can be quite large when the internal energy

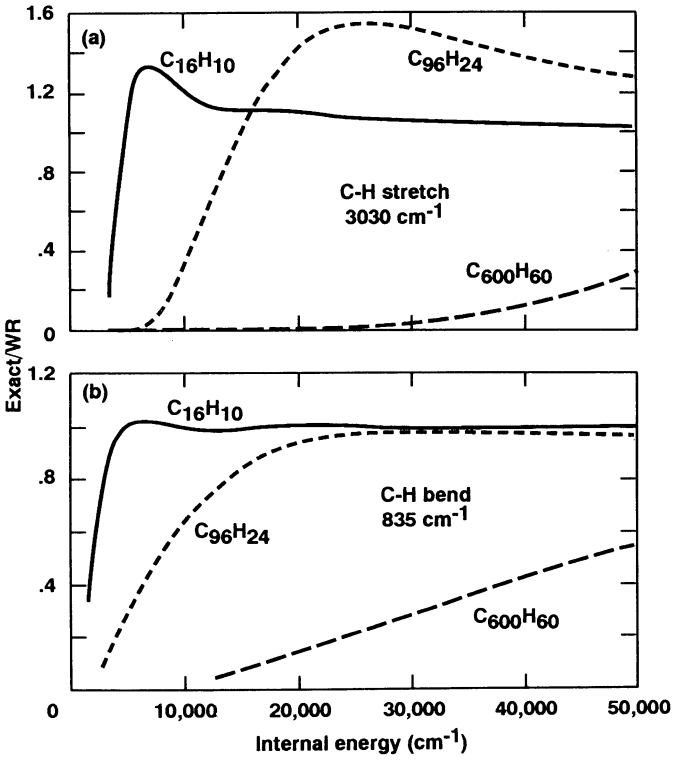

FIG. 2.—Similar to Fig. 1, but with the intensity calculated by the exact method ratioed to the intensity obtained with the WR approximation.

falls below $\sim 30{,}000$ cm^{-1}. This lower internal energy range is quite important in the modeling of the interstellar PAH emission since large PAHs are efficient absorbers at these photon energies (see § 3.2.5). Moreover, and more importantly, during the relaxation phase which follows a photon absorption by small and large PAHs alike, a vibrationally excited PAH will gradually lose its excess energy through IR emission and, hence, will emit a large fraction of its excess energy while in this lower internal energy range. Fortunately, as will be demonstrated below, the presence of a size distribution will alleviate this concern.

To compare the exact with the thermal model, the time-averaged IR emission spectrum from a PAH molecule of type j embedded in a stellar radiation field of blackbody temperature T^* with cutoff at 912 Å (109,600 cm^{-1}) was calculated (i.e., the IR spectrum emitted by a large ensemble of such PAHs exposed to this field). The fraction of the time-averaged total IR flux emitted in the ith mode, $P(j, i)/P(j)$, is given by

$$\frac{P(j, i)}{P(j)} = \int_0^\infty \sigma(\nu) F_*(\nu) \frac{f(j, \nu, i)}{h\nu} d\nu \Big/ \int_0^\infty \sigma(\nu) F_*(\nu) d\nu \quad (10)$$

with

$$f(j, \nu, i) = \int_0^{h\nu} \frac{I(j, E, i)}{I(j, E)} dE , \quad (11)$$

where $I(j, E, i)/I(j, E)$ is the fraction of the total IR intensity emitted by a molecule of type j at internal vibrational energy E in the ith IR-active mode, $f(j, \nu, i)$ is the total energy emitted in the ith mode following the absorption of a UV/visual photon of frequency ν, F_* is the stellar UV/visual flux per unit frequency interval, and $\sigma(\nu)$ is the UV/visual absorption cross section of the molecule. Table 1 compares the fraction of the total IR flux emitted in the 3030 cm^{-1} C—H stretching and in the 835 cm^{-1} C—H out-of-plane bending modes calculated using the exact method with that using the thermal model. For computational reasons, the thermal model has been used to calculate the total IR intensity $I(j, E)$, which has been used to normalize the results of both the exact and the thermal model to the total IR emission. Entries are given for pyrene ($C_{16}H_{10}$), $C_{96}H_{24}$, and $C_{600}H_{60}$ in 5000, 10,000, 40,000, and 100,000 K stellar radiation fields, temperatures which span the range of exciting stars in the objects which emit the interstellar IR bands. The integrated cross sections per H or per C atom used for the IR active modes, and the assumed visual and UV absorption properties are described in § 3.

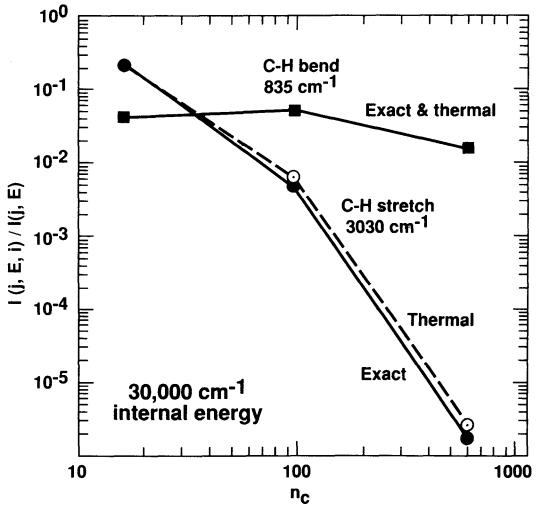

FIG. 3.—Fluorescent emission in the 3030 cm^{-1} and in 835 cm^{-1} bands, divided by the total emission intensity, as a function of the number of C atoms in the PAH. The emission was calculated at vibrational energy $E = 30{,}000$ cm^{-1}. Results obtained with the exact method and with the thermal approximation are shown.

As can be seen from Table 1, the differences between the relative amount of flux in a given IR feature obtained from the thermal and from the exact model are small, i.e., $\sim 3\%$–20%, *as long as a PAH molecule emits appreciable flux in the feature. Larger deviations occur only for PAHs for which the emission in the feature becomes negligibly small.* Thus, when integrating over the size distribution of PAHs, the thermal model will introduce only a small error in the obtained emission spectrum. This is further illustrated in Figure 3, which plots the emission in the 3030 cm^{-1} and in the 835 cm^{-1} features

TABLE 1

INTENSITY OF THE EMISSION IN THE 3030 cm^{-1} AND 835 cm^{-1} FEATURES DIVIDED BY THE TOTAL IR EMISSION (FOR THREE PAHs), CALCULATED BY THE EXACT AND BY THE THERMAL MODEL AS A FUNCTION OF THE RADIATION FIELD TEMPERATURE

	$C_{16}H_{10}$			$C_{96}H_{24}$			$C_{600}H_{60}$		
T (K)	Exact	Thermal	Exact / Thermal	Exact	Thermal	Exact / Thermal	Exact	Thermal	Exact / Thermal
				C—H Stretch (3030 cm^{-1})					
5,000	1.3 (−1)	1.4 (−1)	0.93	7.4 (−4)	9.6 (−4)	0.77	6.1 (−8)	9.6 (−8)	0.64
10,000	1.5 (−1)	1.6 (−1)	0.94	2.3 (−3)	2.7 (−3)	0.86	1.6 (−6)	1.9 (−6)	0.82
40,000	2.0 (−1)	2.1 (−1)	0.97	9.3 (−3)	1.0 (−2)	0.92	2.7 (−5)	3.0 (−5)	0.90
100,000	2.1 (−1)	2.2 (−1)	0.97	1.1 (−2)	1.2 (−2)	0.92	3.4 (−5)	3.8 (−5)	0.90
				C—H Out-of-Plane Bend (835 cm^{-1})[a]					
5,000	5.8 (−2)	6.2 (−2)	0.94	7.0 (−2)	7.5 (−2)	0.93	5.0 (−3)	6.6 (−3)	0.76
10,000	5.6 (−2)	6.0 (−2)	0.95	6.6 (−2)	7.0 (−2)	0.94	8.4 (−3)	1.0 (−2)	0.84
40,000	4.8 (−2)	5.1 (−2)	0.96	5.6 (−2)	5.8 (−2)	0.96	1.3 (−2)	1.4 (−2)	0.92
100,000	4.7 (−2)	4.9 (−2)	0.96	5.4 (−2)	5.6 (−2)	0.97	1.3 (−2)	1.4 (−2)	0.93

[a] Only emission in modes due to two adjacent H atoms are included. There are four, 12, and 12 of such H atoms on $C_{16}H_{10}$, and $C_{96}H_{24}$, and $C_{600}H_{60}$, respectively.

divided by the total IR flux as obtained by the thermal and exact model as a function of PAH size. Values were obtained at $E = 30{,}000\ \mathrm{cm}^{-1}$, roughly corresponding to the average vibrational energy at which interstellar PAHs fluoresce. It can be seen that when integrating the emission in a certain band over a PAH size distribution, the thermal model will introduce only a small error in the outcome, essentially because the error in the calculated band flux is small for PAH sizes that contribute significantly to that particular band.

In summary, *for a size distribution of PAHs*, the errors introduced by using the thermal approximation to calculate the emergent spectrum are less than $\sim 10\%$ in the relative band fluxes. Thus, we have used the thermal approximation in the remainder of the paper.

3. THE INTERSTELLAR PAH EMISSION MODEL

3.1. *Mathematical Formulation*

To model the emission from a size distribution of interstellar PAHs we assume that the PAHs are exclusively excited by one-photon processes, i.e., the interval between successive absorption events of UV/visual photons is sufficiently long that the PAH is able to lose essentially all of its excitation energy by IR fluorescence before absorbing another photon. Under this condition, the IR fluorescence *spectrum* is independent of absolute values of the UV/visual absorption cross sections and flux level. The magnitude of the IR flux does, of course depend on these values. The flux in mode i from a size distribution of PAH molecules in a stellar radiation field is then given by

$$F(i) = \sum_j n_{\mathrm{PAH}}(j) P(j, i)\ , \qquad (12)$$

where $P(j, i)$ is given by equations (10) and (11), $N_{\mathrm{PAH}}(j)$ gives the number density of PAHs of type j, and the summation takes place over all PAHs.

3.2. *Free Parameters*

The free parameters in modeling the interstellar IR emission bands using equations (4), (5), (10), (11), and (12) are the positions, widths, and relative strengths of the IR-active PAH features, the relation between the internal energy and the temperature, the UV/visual absorption properties, the PAH molecular structure, the degree of hydrogenation of the PAHs, their size distribution, and the exciting radiation field. Table 2 gives the adopted standard values for some of these parameters. Below we discuss our choices.

3.2.1. *The PAH Structure*

PAH structure determines the amount of H atoms relative to C atoms in the molecule as well as the number of peripheral H atoms that are isolated, doubly adjacent, or triply adjacent ($n_{\mathrm{H},1}$, $n_{\mathrm{H},2}$, and $n_{\mathrm{H},3}$, respectively). PAH structure will therefore influence the relative strengths of the various C—H and C—C IR active modes.

Comparison of laboratory spectra with observations, and stability considerations, indicate that the interstellar IR emission bands are best reproduced by "compact," symmetric PAH, i.e., PAHs with each aromatic ring part of at least two other aromatic rings (van der Zwet & Allamandola 1985; Cohen et al. 1985; Tielens et al. 1987; Léger et al. 1989a). For disklike, compact PAHs with $n_{\mathrm{C}} \gtrsim 30$, the number of H atoms is, with $\sim 15\%$ accuracy, given by

$$n_{\mathrm{H}} = 2.8\sqrt{n_{\mathrm{C}}}\ . \qquad (13)$$

This expression will somewhat underestimate the number of H atoms if the PAHs are strongly elongated. We further assume $n_{\mathrm{H},1} = n_{\mathrm{H},2} = n_{\mathrm{H},3} = n_{\mathrm{H}}/3$. This holds well for large PAHs ($n_{\mathrm{C}} \gtrsim 100$) but in general somewhat underestimates $n_{\mathrm{H},2}$ and $n_{\mathrm{H},3}$ for smaller molecules (e.g., Stein & Brown 1986; Tielens et al. 1987). For the small PAHs in our model, i.e., coronene ($C_{24}H_{12}$) and pyrene ($C_{16}H_{10}$), exact values for $n_{\mathrm{H},i}$ and n_{C} are used.

3.2.2. *The Degree of Hydrogenation*

It has been suggested that interstellar PAHs are considerably dehydrogenated (Léger & d'Hendecourt 1987; Jourdain de Muizon et al. 1990a). Besides decreasing n_{H} relative to n_{C}, dehydrogenation will also influence the relative values of $n_{\mathrm{H},1}$,

TABLE 2

STANDARD VALUES FOR MODELING THE EMISSION BY INTERSTELLAR PAHS

Parameter	Value
PAH Structure (§ 3.2.1 & 3.2.2):	
Number of H atoms: n_{H}	$2.8 n_{\mathrm{C}}^{0.5}$
Number of single, double, triple, adjacent: $n_{\mathrm{H},i}$ $(i = 1, 2, 3)$	$0.33 n_{\mathrm{H}}$
Fractional H coverage: f_{H}	1.0
Mean radius: $\langle a \rangle$ (Å)	$0.82 n_{\mathrm{C}}^{0.5}$
IR properties (§ 3.2.4):	
Cross section: σ_{C} (cm^2 C-atom^{-1})	See Table 3 (3–15 μm)
	$4.3 \times 10^{-20} (\lambda/\mu\mathrm{m})^{-1.24}$ (≥ 15 μm)
UV/Visual properties (§ 3.2.5):	
Absorption cut-off: λ_c(Å)	$1630 + 450\langle a \rangle$
Cross section: σ_{C}(cm^2 C-atom^{-1})	$4.3 \times 10^{-8}/[5.3 \times 10^{-9} - (\nu_c/\mathrm{cm}^{-1})^2]$ $(\lambda \leq \lambda_c)$
Size distribution (§ 3.2.6):	
B_{C}	3.72×10^{-6}
β	0.833
α	3.5
Smallest PAH: n_{C}(min)	14
Radiation field (§ 3.2.7):	
Effective temperature: T^*(K)	40,000

$n_{H,2}$, and $n_{H,3}$. Assuming that the H atoms are randomly distributed over the available sites, the number of isolated, two adjacent, and three adjacent C—H groups as a function of degree of hydrogenation of the model PAHs are given by

$$n_{H,1}(f_H) = n_H(1)(f_H - \tfrac{7}{9}f_H^2 + \tfrac{1}{9}f_H^3)\,, \quad (14a)$$

$$n_{H,2}(f_H) = n_H(1)(\tfrac{7}{9}f_H^2 - \tfrac{4}{9}f_H^3)\,, \quad (14b)$$

$$n_{H,3}(f_H) = n_H(1)(\tfrac{1}{3}f_H^3)\,, \quad (14c)$$

where f_H is the degree of hydrogenation, i.e., the fraction of the peripheral bonding sites to which an H atom is attached. Figure 4 shows $n_{H,1}$, $n_{H,2}$, and $n_{H,3}$ as a function of f_H. It can be seen that $n_{H,2}$ and especially $n_{H,3}$ decrease rapidly with decreasing f_H, while $n_{H,1}$ decreases much slower and, in fact, initially slightly increases, due to the conversion of adjacent C—H groups to isolated C—H groups by the dehydrogenation process.

Following Tielens et al. (1987) $f_H = 1$, i.e., 100% hydrogenation, is assumed in the standard model. However, models with moderate to severe dehydrogenation are investigated in §§ 4 and 5.

3.2.3. *The Relation between Temperature and Internal Energy*

To fully describe the relation between the total internal vibrational energy and the temperature of a species requires either that the frequencies of all vibrational modes (cf. eq. [5]), or the heat capacity as a function of T, is known. Unfortunately, neither vibrational frequencies nor heat capacities of PAHs larger than hexabenzocoronene ($C_{42}H_{18}$) have been measured in the laboratory or calculated by theoretical modeling. In this section choices for the PAH vibrational frequencies or, alternatively, for the heat capacity are discussed.

Our approach is based upon the well-known extensive theoretical studies of Stein, Golden, & Benson (1977) who analyzed PAH heat capacities. They showed that these heat capacities could be determined in a straightforward manner by simply counting the number of chemical subgroups which made up a particular PAH and summing up the contributions from each group. Extending this concept of similar contributions from

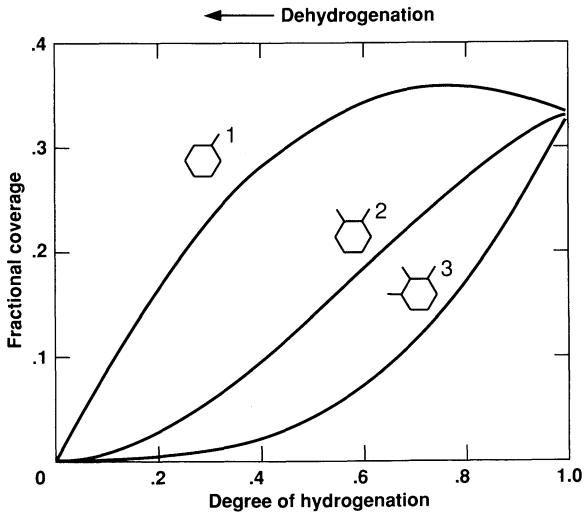

FIG. 4.—The fraction of all peripheral sites occupied by isolated, doubly, or triply adjacent H atoms ($n_{H,1}/n_H$, $n_{H,2}/n_H$, and $n_{H,3}/n_H$, respectively) for a series of compact PAHs as a function of the degree of hydrogenation f_H. Complete hydrogenation corresponds to $f_H = 1$.

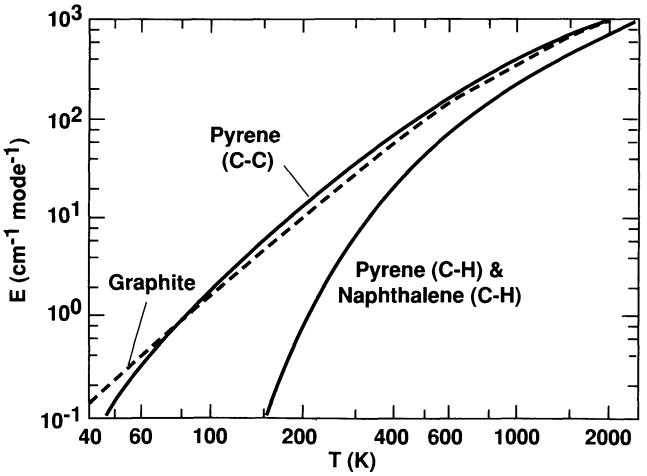

FIG. 5.—Relation between the vibrational energy per mode E_{mode} and the temperature, T, of the material. Shown are the curves obtained for graphite (*dashed line*), for the C—C modes of pyrene (*solid line*), and for the C—H modes of pyrene and naphthalene (*solid line*).

similarities in molecular structure to frequencies, it is expected that the C—C modes of all compact PAHs will have similar frequencies. Figure 5 shows that indeed the temperature dependence of the average energy per mode E_{mode} for the carbon skeleton of the small PAH pyrene, and of graphite are quite similar (cf. Léger et al. 1989a, b who used a similar approach based upon coronene). Following McClellan & Pimentel's vibrational analysis of naphthalene (McClellan & Pimentel 1955), The $3n_C$-6 C—C and $3n_H$ C—H modes of pyrene were distinguished using the vibrational frequencies and the frequency shifts upon deuteration (Bree et al. 1971). The graphite curve was derived from the measurements of the specific heat as a function of temperature (Touloukian & Buyco 1970). There are some small differences. First, for $T \lesssim 80$ K, or, equivalently, $E_{mode} \lesssim 1$ cm^{-1}, the energy per mode for graphite is much larger than for pyrene. This is due to the presence of very low frequency modes in graphite ($\lesssim 100$ cm^{-1}), corresponding to large scale vibrations of the carbon skeleton. Since the frequencies of such vibrations decrease with increasing size of the molecule, larger PAHs will possess modes at lower frequencies than smaller PAHs. Thus, for large PAHs, E_{mode} will fall between the limits provided by pyrene and graphite. Since the low-frequency modes are important only at low temperatures, they do not influence the IR emission from the high-frequency modes ($\nu \gtrsim 400$ cm^{-1}). Second, for $T \gtrsim 80$ K, E_{mode} for graphite is $\sim 15\%$ lower than for the pyrene carbon skeleton. This difference is due to an overall increase of the frequencies of the C—C vibrational modes in graphite due to the rigidity provided by the large lattice. Indeed, by increasing the frequencies by 8%, the pyrene $E_{mode}(T)$ curve can be made to fit the graphite curve above 100 K to within a few percent. A similar difference was reported by Stein et al. (1977).

In our calculations we will use the E_{mode} function of the pyrene carbon skeleton for PAHs with $n_C < 140$, and the graphite relation for larger PAHs. The size roughly corresponds to the transition from compact PAHs with the majority of C atoms completely surrounded by other C atoms, to those which have most C atoms on the periphery of the carbon skeleton (cf. Stein et al. 1977). Assuming that the E_{mode} relation of the carbon skeleton of compact PAHs larger than pyrene falls between those of pyrene and graphite, the error made in

this approach can be evaluated by varying the 140 C atom threshold. When calculating the integrated emission spectrum of a size distribution of PAHs (see § 4 below), variation of the threshold between $n_C = 30$–1500 results in differences in the relative intensity of any emission feature of at most 3%. We conclude therefore that the error introduced by the uncertainty in the E/T relation is negligibly small.

To define the E_{mode} function of the C—H vibrational modes in PAHs we use the C—H vibrational frequencies of pyrene. The resulting curve and, for comparison, the function obtained from the naphthalene C—H modes (McClellan & Pimentel 1955) are shown in Figure 5. The error made adopting this procedure is small relative to the error introduced by the exceedingly small difference between the $E_{mode}(T)$ curves for the C—H modes of pyrene and naphthalene.

3.2.4. *The Infrared Active Modes*

The Einstein A-value of the $v = 1$–0 transition of an IR active mode can be found from the cross section of the mode integrated over the wavelength, $\sigma_{int,i}$, using

$$A_i^{1,0} = \frac{8\pi c}{\lambda_i^4}\,\sigma_{int,i}\,. \tag{15}$$

This section discusses our choices for $\sigma_{int,i}$ as well as for the position and the width of the various IR active modes used in modeling the interstellar PAH emission.

3.2.4.1. The Mid-IR ($3 \leq \lambda \leq 15$ μm)

Positions and widths of the infrared active modes between 3 and 15 μm have been adopted from observations of the interstellar IR emission bands (Table 3). Observed positions and widths are preferred since there are, in general, slight discrepancies in position and considerable discrepancies in width with laboratory measurements of PAHs (Schutte et al. 1990). These discrepancies are possibly due to differences between the conditions in space and in the laboratory (i.e., PAH size, ionized vs. neutral PAHs, gas phase PAHs vs. PAHs in KBr or KI pellets, emission spectra vs. absorption spectra, etc.). Moreover, the interstellar emission bands will be broadened due to the sloshing around of the energy between different vibrational modes (Heisenberg uncertainty relation; $\Delta E\,\Delta t \geq \hbar$ and because of overlap of the features from a wide variety of PAHs. Using the observed position and widths therefore facilitates the comparison between the model emission spectrum and the observations. However, for the coupled C—H out-of-plane bending modes of two adjacent and of three adjacent H atoms laboratory positions were adopted (11.95 and 13.30 μm, respectively), since no unequivocal identification of an interstellar band with these modes has been made. An emission band which is observed at 12.7 μm toward a number of sources could be due to either of these modes (Cohen et al. 1985; Roche et al. 1989; Witteborn et al. 1989).

Table 3 lists two sets of integrated cross sections for the IR active modes. The first set is based on laboratory measurements of small PAHs ($10 \leq n_C \leq 24$) in the gas phase or frozen in neon matrices (see Schutte et al. 1990, and references therein). The second set, which is used in our standard model, has enhanced cross sections for the 6.2, 7.7, and 6.8 μm bands. The strength of an IR mode of a PAH is then found by multiplying its listed integrated cross sections by n_C for C—C modes and by n_H for C—H modes.

3.2.4.2. The Far-IR ($15 \leq \lambda \leq 100$ μm)

The far-IR vibrational modes of PAHs originate from large-scale out-of-plane motions of the carbon skeleton. Far-IR absorption spectra out to ~100 μm have been measured in the laboratory in KI, KBr, and polyethylene pellets of a number of PAHs of size between 14 and 42 C atoms (Léger et al. 1989a; Donn 1988; Donn, Allen, & Khanna 1989; Wdowiak 1989; Cyvin & Klaeboe 1988; Sadtler Atlas of IR Spectra 1966). The position of these modes depends sensitively on the molecular structure. Thus emission from a broad size distribution of PAHs would tend to produce a "quasi continuum" when measured under low spectral resolution (ATB). The average far-IR cross section is plotted as a function of wavelength in Figure 6. Since not all available spectra extend to 100 μm, the average

TABLE 3

POSITIONS, WIDTHS, AND INTEGRATED CROSS SECTIONS FOR THE PAH MID-IR ACTIVE MODES ADOPTED IN THE MODEL CALCULATION

VIBRATION	POSITION[a] (μm)	FWHM[a] (μm)	INTEGRATED CROSS SECTION (σ_{int})[b] (cm² μm)	
			Laboratory[d]	Standard
C—H stretch	3.295	0.048	1.4 (−21)	1.4 (−21)
C—C stretch	6.18	0.24	7.6 (−22)	1.8 (−21)
C—C stretch	7.62	0.20+0.60[c]	2.0 (−21)	1.2 (−20)
C—H bend (in-plane)	8.60	0.28	1.0 (−21)	6.0 (−21)
C—H bend (out-of-plane):				
Isolated C—H	11.26	0.16	4.0 (−20)	4.0 (−20)
Two adjacent C—H	11.95[d]	0.29[e]	1.9 (−20)	1.9 (−20)
Three adjacent C—H	13.30[d]	0.29[e]	1.9 (−20)	1.9 (−20)

[a] Adopted from observations of the IR emission bands toward Orion position 4 (Geballe et al. 1989; Bregman et al. 1989; Roche et al. 1989), unless otherwise noted.

[b] Integrated cross sections are given per H atom for C—H vibrational modes and per C atom for C—C modes.

[c] The observed 7.7 μm feature is strongly asymmetric. Entries give the adopted width of the short-wavelength and the width of the long-wavelength component of the feature, respectively. Their sum is equal to the FWHM of the entire feature.

[d] From laboratory measurements for small neutral PAHs (10–24 C atoms; Schutte et al. 1990, and references therein).

[e] Width of the 12.7 μm emission feature toward Orion position 4 (Roche et al. 1989).

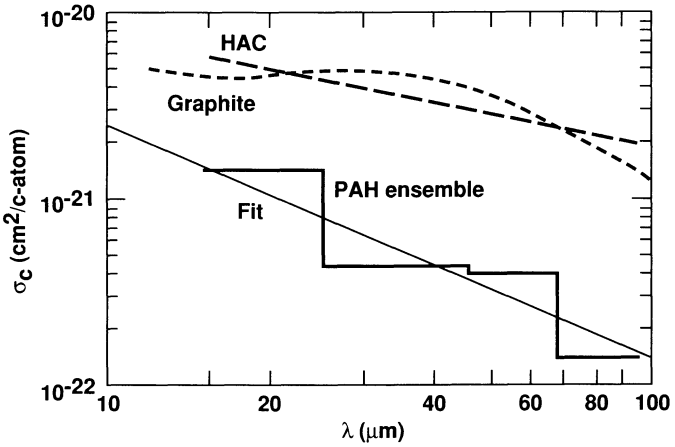

FIG. 6.—The average far-IR absorption cross section as a function of wavelength for an ensemble of PAHs containing between 14 and 42 C atoms (*thick line*). Superposed is the least-squares fit to these data (*thin line*). For comparison, the cross sections measured for hydrogenated amorphous carbon (*long dashed line*; from Tanabé et al. 1983) and for graphite (*short dashed line*; from Draine 1984) are also shown.

cross section in longer wavelength intervals was obtained from a smaller PAH sample. In modeling the emission from interstellar PAHs, the least-squares fit to these data, given by

$$\sigma_C(\lambda) = 4.3 \times 10^{-20}\left(\frac{\lambda}{\mu m}\right)^{-1.24} \text{ cm}^{-2} \text{ per C atom}, \quad \lambda \geq 15\ \mu m \quad (16)$$

and shown in Figure 6 as a straight solid line, was used. This result is slightly different from the relation derived by Leger et al. (1989a) which was based on a somewhat smaller data set. Our adopted cross sections are smaller by 35% at 15 μm to a factor of 2 at 80 μm.

For comparison, the cross section of a hydrogenated amorphous carbon (HAC) material (from Tanabé et al. 1983) and of graphite (Draine 1985) is also displayed in Figure 6. Some clear differences between the FIR absorption properties of these materials are apparent. First, the HAC absorbs considerably stronger than the PAH sample, i.e., 4 times at 16 μm. Other amorphous carbon or HAC materials produced in the laboratory by various techniques were found to have even larger far-IR cross sections (Bussoletti et al. 1987). Furthermore, the cross section of the PAH sample decreases as $\lambda^{-1.24}$, while for the HAC it scales with $\lambda^{-0.59}$, and for graphite it is approximately constant out to 50 μm. In contrast to PAHs, all modes are somewhat IR active in a disordered material such as HAC. This leads to a general increase in the absorption cross section. Moreover, a macroscopic material will have modes (i.e., phonons) at much lower frequencies than PAHs. Finally, for graphite, a semimetal, the IR absorption is dominated by electronic transitions, not vibrations. Indeed, for such a well-ordered material, the vibrational modes are very weak compared to the continuum (Draine 1984). In general, it should be emphasized that the FIR absorption properties of graphite and HAC-related materials form a poor approximation to those of PAHs.

3.2.5. *The UV/Visual Absorption Properties*

PAHs have three absorption band systems in the UV and visible regions. The longer wavelength α and *p* systems are generally much weaker than the shortest wavelength β system (Clar 1952; Jaffé & Orchin 1962) and can be neglected for our purpose of modeling the UV/visual absorption of interstellar PAHs. The β band system is, in general, characterized by a sharp cutoff, which shifts to longer wavelengths with increasing PAH size (Clar 1952; Platt 1956). Figure 7 shows the measured cutoff wavelength as a function of average size $\langle a \rangle$ for "compact" PAHs (Gutfreund & Little 1969). $\langle a \rangle$ is defined as the radius of a circle of surface area equal to the molecule. With the surface area of an aromatic ring equal to 5.2 Å^2, $\langle a \rangle$ is given by

$$\langle a \rangle = 1.29\sqrt{n_R}\ \text{Å}, \quad (17)$$

where n_R is the number of aromatic rings.

Theoretically, a linear relationship is expected between λ_c and $\langle a \rangle$ for compact PAHs (Robertson 1986). We will therefore use the least-squares fit through the data points displayed in Figure 7 to define the cutoff wavelength for the UV/visual absorption by our model PAHs. This relation is given by

$$\lambda_c = 1630 + 450\langle a \rangle\ \text{Å}. \quad (18)$$

To evaluate λ_c from equations (17) and (18) for large PAHs, we furthermore need a relation between n_R and n_C. For compact, circularly symmetric PAHs with $30 \leq n_C \leq 30{,}000$ this is, with 20% accuracy, given by

$$n_R \approx 0.40 * n_C. \quad (19)$$

The relation between n_C and λ_c given by equations (17), (18), and (19) is shown in Figure 7. It can be seen that although small PAHs ($n_C \lesssim 40$) exclusively absorb in the UV, in this model larger PAHs also absorb in the visual, while extremely large PAH ($n_C \gtrsim 1000$) absorb in the near-infrared as well.

Following ATB, we adopt a constant cross section equal to $\sigma_C = 1 \times 10^{-17}$ cm^2/C atom shortward of the cutoff wavelength for small PAHs ($n_C \approx 24$). Scaling factors for this cross section with PAH can be determined from the requirement that one effective π electron contributes to the excitation between 9.3 eV (72,600 cm^{-1}) and the low-energy cutoff

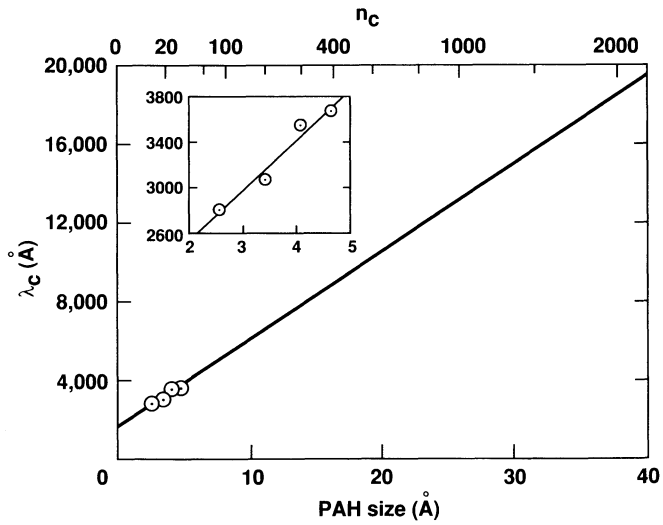

FIG. 7.—Relation between the cutoff wavelength λ_c of the UV/visual absorption, the average PAH size $\langle a \rangle$, and the number of atoms in the carbon skeleton n_C. The data points were obtained for pyrene ($C_{16}H_{10}$), coronene ($C_{24}H_{12}$), ovalene ($C_{32}H_{14}$) and hexabenzocoronene ($C_{42}H_{18}$). Superposed is the least-squares fit through these data.

(Robertson 1986). This results in

$$\sigma_C(\nu_p^2 - \nu_c^2) = \text{constant} , \quad (20)$$

where ν_c is the cutoff frequency ($=\lambda_c^{-1}$) and $\nu_p = 72{,}600\ \text{cm}^{-1}$. It must be noted that equation (20) gives a nearly size independent absorbtivity shortward of the cutoff wavelength. For example, using equations (17), (18), (19), and (20) it is found that the cross section per C atom in the infinitely large size limit is only 20% lower than for coronene ($C_{24}H_{12}$).

3.2.6. *The Size Distribution*

We assume that the PAH size distribution is given by a power law. For our purposes the most convenient form of this law is given by

$$\left(\frac{dN_{\text{PAH}}}{N_H}\right) = B_C n_C^{-\beta-1}\, dn_C \quad n_C \geq n_C(\text{min}) , \quad (21)$$

where $[dN_{\text{PAH}}/N_H]$ is the total number of PAHs per interstellar H atom containing between n_C and $n_C + dn_C$ carbon atoms.

In the classical MRN size distribution, the number of interstellar graphite grains of radius a is given by (Mathis, Rumpl, & Nordsieck 1977; Draine & Lee 1984

$$\left(\frac{dN}{N_H}\right) = A_C a^{-\alpha} da \quad a_{\text{min}} < a < a_{\text{max}} , \quad (22)$$

where $[dN/N_H]$ is the number of graphite grains per interstellar H atom with radius between a and $a + da$, $\alpha = 3.5$, $A_C = 6.92 \times 10^{-26}\ \text{cm}^{\alpha-1}$, $a_{\text{min}} \approx 0.005\ \mu\text{m}$, and $a_{\text{max}} \approx 0.25\ \mu\text{m}$. In our standard model we will extrapolate this relation for particles containing 10^5–10^{10} atoms to the 10–10^4 atom size range relevant to modeling the IR emission features. Using

$$n_C = \frac{4\pi a^3 \rho_{\text{gr}}}{3 m_C} , \quad (23)$$

we then find

$$\beta = \frac{\alpha - 1}{3} \quad (24)$$

$$B_C = \frac{A_C}{3}\left(\frac{4\rho_{\text{gr}}\pi}{3m_C}\right)^{\beta} , \quad (25)$$

where m_C is the mass of the carbon atom, and ρ_{gr} is the density of graphite ($2.26\ \text{g cm}^{-3}$). This yields $\beta = 0.833$ and $B_C = 1.24 \times 10^{-6}$. In the standard model we furthermore adopt $n_C(\text{min}) = 14$.

Désert et al. (1990) described the mid- and far-IR emission using a particle population which is rather different from ours. In their model, the emission originates from two components, i.e., a PAH size distribution given by

$$dN_{\text{PAH}} = a_{\text{PAH}}^{-\gamma} da \quad \text{with} \quad a_{\text{min}} \leq a \leq a_{\text{max}} , \quad (26)$$

where a_{PAH} is the PAH radius, $\gamma = 2$ (corresponding to $\alpha = -2.5$), $a_{\text{min}} = 4$ Å, and $a_{\text{max}} = 10$ Å (corresponding to $n_C \approx 20$ and ≈ 150, respectively). The second component consists of spherical, very small grains (VSGs) with an amorphous carbon-like composition. This component is comprised of particles containing essentially between 10^3 and 10^4 C atoms (the abundance of VSGs with less than 10^3 C atoms is very small). We preferred instead to use a continuous size distribution since there are no clear observational or theoretical grounds for the discontinuity introduced by Désert et al. Moreover, in our model we do not use amorphous carbon particles (i.e., clustered aromatic structures cross-linked by aliphatic chains) but only "flat," free PAHs, since using such particles would introduce a number of ill-defined free parameters. Instead, in § 5.7, we qualitatively discuss the influence that the presence of such particles would have on the model results.

3.2.7. *The Radiation Field*

We will adopt a stellar blackbody with cutoff at 912 Å for the radiation field exciting the PAHs. Thus, since only the spectral shape and not the absolute flux influences the spectral distribution of the fluorescence under the assumption of 1 photon excitation, the only free parameter related to the radiation field is the effective temperature of the exciting star T^*. As standard value we adopt $T^* = 40{,}000$ K, the effective temperature of Θ^1 Ori C, the star illuminating the Orion Bar (Geballe et al. 1989).

4. MODEL SPECTRA

Figures 8*a*–8*j* show the model emission spectra from a size distribution of PAHs obtained for the standard model and by varying the free parameters discussed in § 3 one by one. To obtain the emission integrated over the size distribution, model spectra were calculated for pyrene ($C_{16}H_{10}$), coronene ($C_{24}H_{12}$), and for the hypothethical interstellar PAHs with $n_C = 36$, 54, 82, 126, 196, 294, 420, 600, 1000, 2000, 4000, 8000, 16,000, and 32,000, whose properties were described in § 3. Table 4 lists, for each of the integrated spectra, the calculated ratio expected in the *Infrared Astronomical Satellite* (*IRAS*) 12 and 25 μm band fluxes.

4.1. *The Standard Model*

Figure 8*a* shows the model emission spectrum from a size distribution of interstellar PAHs calculated using the standard values of the free parameters (§ 3, Table 2). The 7.7 μm and the combined out-of-plane modes at 11.3, 12.0, and 13.3 μm give similar contributions to the *IRAS* 12 μm band flux, while the 8.6 μm feature gives a relatively smaller contribution. The 25 μm *IRAS* band flux originates exclusively from far-IR modes.

The flux emitted in the various features and in the *IRAS* 25 μm band is shown in Figure 9 as a function of the PAH size. The various mid-IR features and the far-IR continuum originate from distinctly different PAHs. Features at shorter wavelength are emitted by smaller PAHs. These attain higher

TABLE 4

RATIO OF THE *IRAS* 12 AND 25 MICRON PHOTOMETRIC BAND FLUXES FOR A NUMBER OF MODEL SPECTRA

Model	$F(12)/F(25)$	Corresponding Figure
Standard	1.18	8*a*
$\alpha = 2.5$	0.46	8*b*
$\alpha = 4.5$	2.94	8*c*
$n_C(\text{min}) = 44$	0.92	8*d*
$T^* = 10{,}000$ K	0.79	8*e*
Neutral PAH cross sections	1.02	8*f*
Far-IR: large σ	0.40	8*g*
Far-IR: small σ	2.75	8*h*
$f_H = 0.50$	0.99	8*i*
$f_H = 0.05$	0.69	8*j*
$T^* = 10{,}000$ K; $\alpha = 2.5$	0.36	
$T^* = 10{,}000$ K; $\alpha = 4.5$	1.65	
Neutral PAH cross sections: $f_H = 0.05$	0.36	11

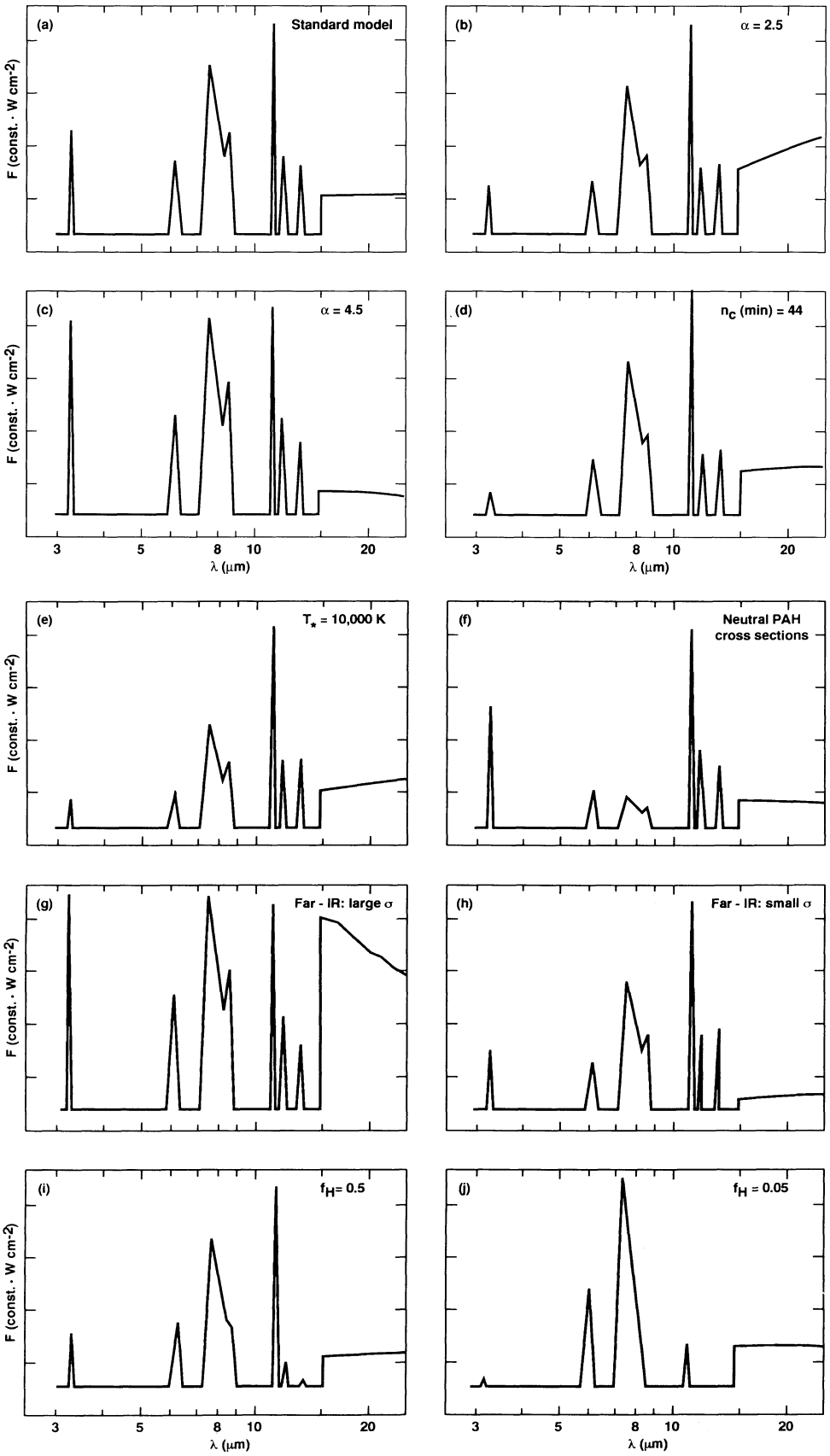

FIG. 8.—Model emission spectra calculated for a size distribution of PAHs embedded in a stellar radiation field. Each parameter has been varied independently. The parameters for the standard model are given in Table 2.

(*a*) Standard model; (*b*) $\alpha = 2.5$; (*c*) $\alpha = 4.5$; (*d*) $n_C(\text{min}) = 44$; (*e*) $T^* = 10{,}000$ K; (*f*) laboratory mid-IR cross sections (Table 3); (*g*) 10 times larger far-IR cross sections; (*h*) 10 times smaller far-IR cross sections; (*i*) $f_H = 0.50$; (*j*) $f_H = 0.05$.

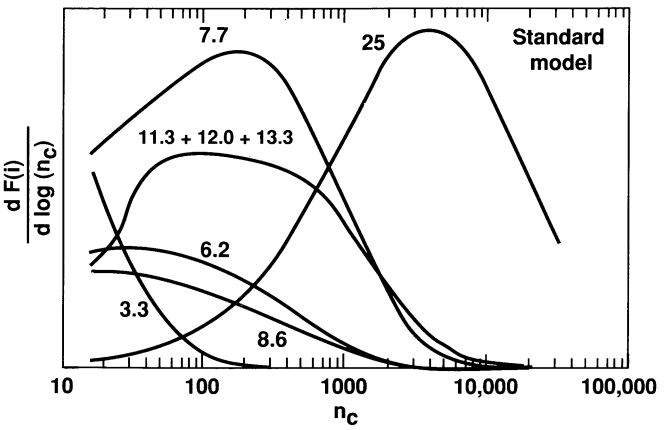

FIG. 9.—Contribution to the total emission in a feature, $dF/d\ln(n_C)$, as a function of the PAH size (i.e., the number of C atoms n_C), for the mid-IR features and for the *IRAS* 25 μm photometric band, in the standard model. The surface area under each of curve gives the total flux emitted in the corresponding IR feature.

excitation levels after absorbing a photon. Furthermore, at similar wavelengths, C—H modes are emitted by somewhat smaller PAHs than the C—C modes, since the number of H atoms relative to C atoms in a model PAH decreases with size as $n_C^{-0.5}$ (eq. [13]).

4.2. *The Size Distribution* [α, n_C(min)]

Figures 8*b*, 8*c*, and 8*d* show the model emission spectra obtained by varying the size distribution. Increasing the amount of larger PAHs ($\alpha = 2.5$) enhances the relative emission from longer wavelength features (Fig. 8*b*). Conversely, the shorter wavelength bands are enhanced with $\alpha = 4.5$ (Fig. 8*c*). The influence of α is especially pronounced in the ratio of the 3.3 μm band to the other mid-IR features and in the relative intensity of the mid- and far-IR emission. This reflects the differences in the sizes of the PAHs responsible for the bulk of emission in these regions (Fig. 9). The 8.6/7.7 μm ratio also varies somewhat with α. The influence on the 11.3/7.7 μm ratio is, on the other hand, rather small.

Increasing the minimum PAH size to n_C(min) = 44 leads to a strong decrease of the 3.3 μm feature (Fig. 8*d*). The influence on the relative intensities of the other features is small, since PAHs with $n_C \leq 44$ contribute little to these bands.

4.3. *The Radiation Field Temperature* (T^*)

Figure 8*e* shows the model emission spectrum obtained for an exciting radiation field of temperature $T^* = 10{,}000$ K. At this lower temperature the shorter wavelength features decrease in the intensity relative to the longer wavelength features. This is related to two effects. First, due to the lower average photon energy, the average emission temperature of a given PAH is lower. Second, because the UV/visual absorption threshold wavelength λ_c increases with PAH size (§ 3.25), the relative contribution to the emission from smaller, hotter, PAHs decreases in the cooler radiation field.

4.4. *The Integrated Cross Section of the* 6.2, 7.7, *and* 8.6 *Micron Features*

Figure 8*f* shows the model emission obtained using the integrated IR cross sections that have been measured for small, neutral PAHs (Table 3). As expected, this decreases the relative intensity of the 6.2, 7.7, and 8.6 μm bands. The ratio of the intensities of the 7.7/11.3 μm features, for example, decreases by a factor 5.2, close to the decrease in the ratio of their intrinsic strengths. The relative intensities of the other emission features change little as compared to the standard model.

4.5. *The Far-IR Absorption Cross Sections*

Figure 8*g* shows the model spectrum obtained using 10 times larger far-IR cross sections than in the standard model. As expected, the intrinsic strengths of the far-IR modes have considerable influence on the far-IR emission level. This also influences somewhat the relative distribution of the mid-IR features. The intensity of the 3.3 μm feature strongly increases relative to the longer wavelength mid-IR features, while there is a small increase in the 7.7/11.3 μm ratio. This can be ascribed to the additional far-IR emission originating from PAHs at temperatures at which the 7.7 μm mode and the out-of-plane modes also emit intensely. The 3.3 μm band is emitted at temperatures where far-IR emission is almost negligible. Thus the gain in the far-IR flux is primarily at the expense of the longer wavelength mid-IR bands. Conversely decreasing the far-IR cross sections by a factor of 10 constrains the relaxation to the mid-IR and increases the relative flux in the 7.7 μm and the out-of-plane bending features with respect to the 3.3 μm band (Fig. 8*h*).

4.6. *The Degree of Hydrogenation*

Figures 8*i* and 8*j* show the model spectra obtained with 50% and 5% hydrogenated PAHs, respectively. As expected, the dehydrogenated PAHs emit less flux in the 3.3 μm, 8.6 μm, and the combined out-of-plane C—H bending features. However, for the 50% hydrogenated model, the 11.3/7.7 μm intensity ratio does not change significantly with respect to the standard model. This is due to the conversion by the dehydrogenation of C—H groups in ensembles of 2 or 3 adjacent C—H groups to isolated groups, counteracting the effect of the overall loss of hydrogen atoms (§ 3.2.2, Fig. 4). However, due to the fast disappearance of ensembles of adjacent C—H groups, the 12.0 and especially the 13.3 μm feature diminish strongly upon dehydrogenation. Fifty percent dehydrogenation results in a strong reduction of the 12.0 μm feature and the virtual disappearance of the 13.3 μm feature, while at 5% hydrogenation, only the 11.3 μm feature remains.

5. THE OBSERVED IR EMISSION BANDS AND THE PROPERTIES OF INTERSTELLAR PAHS

5.1. *IR Spectra toward a Number of PAH Emission Sources*

Four PAH emission objects have been especially well studied in the 2.8–13 μm region. These are the planetary nebulae BD 30°3639 and NGC 7027, the proto–planetary nebula HD 44179, and position 4 in the Orion Bar. We have collected the various data sets available for these objects in order to synthesize the emission spectrum of each object across the entire mid-IR spectral region. Where possible, IR emission features in low-resolution spectra have been replaced by recent high-resolution data, scaling by the ratio of the integrated strength of the features in both spectra. In the case of the Orion Bar, where the PAH emission is very extended (e.g., Geballe et al. 1989; Roche et al. 1989), we reduced all spectral data to the emission level at a fixed aperture of 5″ around position 4 using photometric data as a guide. The results are shown in Figure 10.

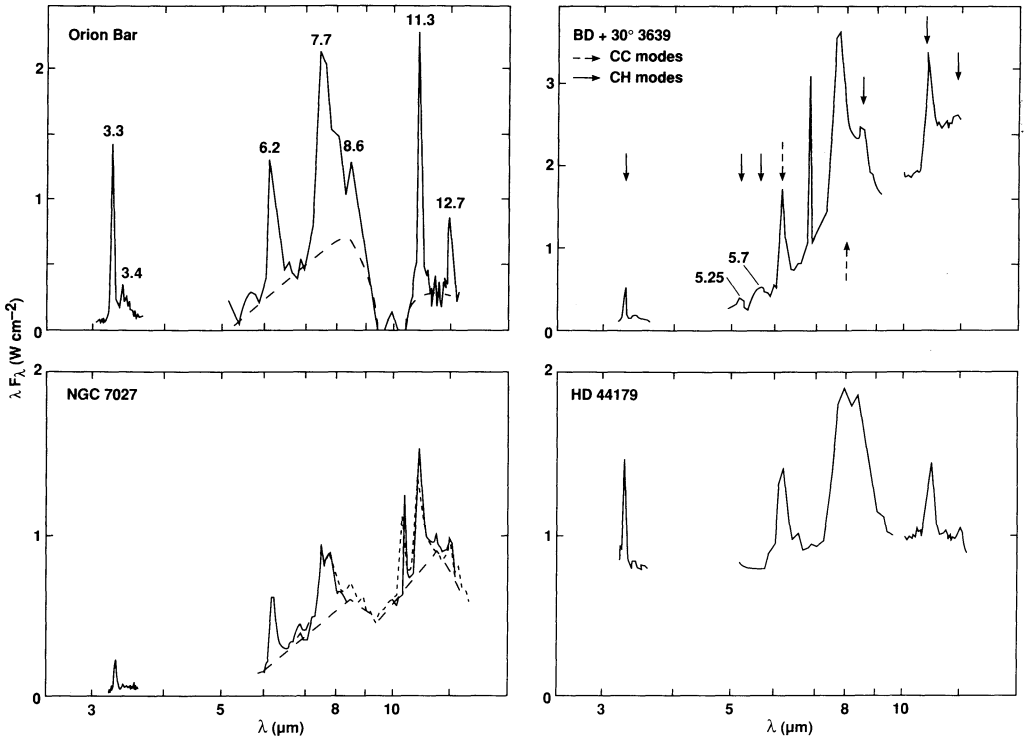

FIG. 10.—The emission spectra toward position 4 in the Orion Bar, BD +30°3639, NGC 7027, and HD 44179. All data have been scaled to a 5″ aperture. Intensity axes are 10^{-16} W cm^{-2} for Orion and NGC 7027, 10^{-15} W cm^{-2} for BD +30°3639, and 10^{-14} W cm^{-2} for HD 44179. Note that the wavelength axes are on a log scale. For details and references, see text. Arrows and peak wavelengths designate the interstellar infrared emission features attributed to free PAH molecules. The long dashed lines underlying the features in the spectra toward Orion and NGC 7027 indicate the contribution from larger PAHs and PAH clusters.

The planetary nebula BD 30°3639 has a diameter of about 6″ (Hora et al. 1990). Spectra of the entire nebula are available between 4.9 and 9.2 μm from Allamandola et al. (1989b; 27″ aperture), between 10.1 and 12.5 μm from Witteborn et al. (1989; 12″ aperture). The 12.5–13.1 μm portion of this spectrum is omitted in Figure 10 because it is dominated by Ne II emission at 12.5 μm), and finally between 2.9 and 9.4 μm from the low-resolution data of Russell, Soifer, & Merrill (1977a; 17″ aperture). The low-resolution data was augmented by the 3.2–3.6 μm spectrum from Geballe et al. (1989; 5″ aperture) using a scaling factor of 1.75.

The planetary nebula NGC 7027 has a maximum diameter of about 12″ (Arens et al. 1984). The 2.9–4.1 μm spectrum of Merrill, Soifer, & Russell (1975; 17″ aperture) has been appended by the 3.2–3.6 μm spectrum of Nagata et al. (1988); 2.7″ aperture), scaled by a factor of 16.3. The 5.0–8.0 μm portion of the spectrum is taken from Bregman et al. (1989). The low resolution 7.5–13.7 μm data of Russell et al. (1977b; aperture 17″ [*short-dashed line*]) has been partially replaced by the 10.1–13.0 μm high-resolution spectrum of Witteborn et al. (1989; 12″ aperture [*solid line*]), scaled by a factor of 1.68.

The maximum diameter of the protoplanetary nebula HD 44179 is about 4″ (Russell, Soifer, & Willner 1978). The low-resolution 2.9–4.1 μm data from Russell et al. (1977a; aperture 17″) has been augmented by the high-resolution study of Geballe et al. (1989; aperture 5″). The 5–13 μm spectra are from Cohen et al. (1986; aperture 21″) and Witteborn et al. 1989; aperture 12″), with the latter scaled to the former by 1.13 to match the flux in the 11.2 μm feature.

All data for Orion position 4 were scaled to the 5″ aperture of the 3.0–3.7 μm spectrum measured by Geballe et al. (1989). First, the 5.2–12.3 μm spectrum from Bregman et al. (1989; 21″ aperture) was scaled to the 6″ 11.0–13.2 μm spectrum reported by Roche et al. (1989) using a factor of 0.17 to match fluxes in the 11.2 μm band. These data were then smoothed to a resolution of 1.2 μm to compare with photometric measurements at 8.7, 9.5, and 11.2 μm of Becklin et al. (1976; aperture 4″.5). This indicated that a scaling factor of about 0.6 was needed to adjust the level of the 5.2–13.2 μm spectrum to the level of the 3.0–3.7 μm spectrum.

5.2. *The Radiation Field in the Emission Objects*

Since our model assumes that the PAHs are excited by one-photon processes, we assessed the validity of this assumption for a number of interstellar environments where the IR emission bands are observed. According to Figure 9, the mid-IR bands are predominantly emitted by PAHs with less than ~1000 C atoms. Thus, multiphoton processes do not influence the distribution of the mid-IR emission as long as the one-photon assumption holds for these PAHs. Photon fluxes and photon absorption rates are given in Table 5 for the emission sources of Figure 10. It can be seen that for the objects with circumstellar PAHs—BD 30°3639, NGC 7027, and HD 44179—multiphoton processes are important even for PAHs containing less than 10^3 carbon atoms, implying that the relative intensities of the mid-IR bands will be influenced. Caution should therefore be used in applying our model to the observations of these objects. For position 4 in the Orion Bar, on the other hand, multiphoton processes become important only for $n_C \gtrsim 10^3$, and the one-photon assumption can therefore be used for modeling its mid-IR emission spectrum. For the diffuse medium, the one-photon assumption holds out to $n_C \approx$

TABLE 5

FLUX LEVELS, PHOTON ABSORPTION RATES, AND THE NUMBER OF PHOTON ABSORPTION EVENTS PER RELAXATION PERIOD FOR SOME PAHs IN VARIOUS OBJECTS

OBJECTS	PHOTON FLUX[a] (cm^{-2} s^{-1})	ABSORBED[a] Photons s^{-1}				Photons/(Relaxation Time)[b]			
		$C_{16}H_{10}$	$C_{96}H_{27}$	$C_{600}H_{69}$	$C_{32000}H_{501}$	$C_{16}H_{10}$	$C_{96}H_{27}$	$C_{600}H_{69}$	$C_{32000}H_{501}$
HD 44179	1.6 (15)[c]	6.6 (−2)	1.3	7.9	4.1 (2)	9.0 (−2)	4.6	1.3 (2)	2.1 (5)
NGC 7027	1.7 (14)[d]	2.6 (−2)	1.4 (−1)	8.2 (−1)	4.3 (1)	3.5 (−2)	4.9 (−1)	1.3 (1)	2.2 (4)
BD 30°3639	4.6 (13)[e]	5.9 (−3)	3.8 (−2)	2.3 (−1)	1.2 (1)	8.0 (−3)	1.3 (−1)	3.6	6.2 (3)
Orion Bar	1.1 (13)[c]	1.5 (−3)	8.7 (−3)	5.2 (−2)	2.7	2.0 (−3)	3.1 (−2)	0.82	1.4 (3)
Diffuse ISM	5.9 (8)[f]	2.4 (−8)	4.7 (−7)	2.9 (−6)	1.5 (−4)	3.3 (−8)	1.7 (−6)	4.6 (−5)	8.0 (−2)

[a] From 20,000 to 109,650 cm^{-1}.

[b] Relaxation times from 109,650 to 20,000 cm^{-1} are equal to 1.4, 3.5, 15.9, and 520 s for $C_{16}H_{10}$, $C_{96}H_{10}$, $C_{96}H_{27}$, $C_{600}H_{69}$, and $C_{32000}H_{501}$, respectively.

[c] From Geballe et al. 1989.

[d] Using a total flux of 2×10^{-14} W cm^{-2}, a temperature of 200,000 K (Pottasch 1984), and an angular distance between stellar source and planetary nebula of 2″ (Arens et al. 1984).

[e] Using a total flux of 5×10^{-15} W cm^{-2}, a temperature of 31,000 K (Pottasch 1984), and an angular distance between stellar source and planetary nebula of 2″ (Hora et al. 1990).

[f] The interstellar radiation field is approximated as a blackbody of temperature 10,000 K multiplied by 1×10^{-14} (Spitzer 1978).

10^5, and the model can, in this case, be used at least out to 25 μm. We will therefore use the mid-IR emission spectrum toward Orion position 4 and the 12 and 25 μm observations by *IRAS* of diffuse cirrus clouds with our model to study the properties of interstellar PAHs.

Figure 10 and Table 5 show an inverse correlation between the incident UV/visual flux and the observed IR feature-to-continuum ratio. In the Orion Bar where multiphoton processes are probably unimportant for the mid-IR emission, there is little or no continuum emission present under the emission features. When the incident UV/visual flux increases, multiphoton processes become important for large PAHs (BD 30°3639 and NGC 7027) and the IR continuum rises at the longer wavelength side of the mid-IR region. For HD 44179, where multiphoton processes are important for nearly all size PAHs and thus contribute through the entire mid-IR region, a strong continuum underlies the entire mid-IR spectrum. This suggests that, in these high-flux regions, the continuum emission originates from relatively large species. In spectral regions where emission by multiphoton excited particles is important, large particles will contribute to the mid-IR emission as well as small particles and molecules. Thus PAHs ($n_C < 1000$) emit the IR features, while larger particles ($n_C \gg 1500$) likely emit the underlying continuum in high-flux regions.

5.3. *Comparison of the Orion Bar Spectrum with the Standard Model*

Comparing Figures 8*a* and 10 shows that the standard model fits the relative intensities of the Orion Bar IR emission quite well. The interstellar 12.7 μm feature falls between the 12.0 and 13.3 μm laboratory bands associated with the out-of-plane modes of two and three adjacent H atoms (Table 3). As 12.7 μm is somewhat closer to the three adjacent H atom region, an assignment to this mode was earlier proposed (Roche et al. 1989). However, in this case the absence of an emission feature due to the mode of two adjacent H atoms seems somewhat puzzling. In principle, the continuum emission between 11.5 and 12.6 μm could well be due to such groups (Cohen et al. 1985). However, in Orion, this continuum emission does not spatially correlate with the 11.3 and 12.7 μm features (Roche et al. 1989; Witteborn et al. 1989), and it is therefore likely not due to the PAHs that emit these bands but possibly to large PAHs and PAH clusters (Bregman et al. 1989).

The standard model reproduces the relative intensity of the observed IR emission bands with integrated cross sections for the 6.2, 7.7, and 8.6 μm bands which are enhanced with respect to the laboratory values for neutral PAHs by factors of 2.4, 6.0, and 6.0, respectively. This enhancement in the intrinsic strength of the features is necessary to get a good fit to the observations, and this forms one of the important conclusions of this study. In the remainder of this section, we will discuss briefly the uncertainty introduced by other parameters in the determination of these enhancement factors.

An error in these cross sections is introduced by the uncertainty in the adopted size distribution, the error in the far-IR absorption properties, the assumed molecular structure and possibly by the assumption of 100% hydrogenation. It can be seen from Figures 8*b*, 8*c*, and 8*d* that even considerable variation of the size distribution only slightly influences the 7.7/11.3 μm emission ratio. For example, using alternatively $\alpha = 4.5$ with $n_C(\min) = 20$ results in an identical 3.3/11.3 μm intensity ratio with a 1% larger 7.7/11.3 μm ratio and 10% larger 6.2/11.3 μm and 8.6/11.3 μm ratios as compared to the standard model. The error introduced by the uncertainty in the far-IR absorption properties is likewise rather small. From Figures 8*g* and 8*h* it can be seen that even large variations in the strength of the far-IR absorption bands only leads to a small change in the 7.7/11.3 μm ratio. For example, a model with 10 times larger far-IR absorption, $n_C(\min) = 32$, and $\alpha = 3.5$ reproduces the standard 3.3/11.3 μm ratio with 10% larger 7.7/11.3 μm and 8.6/11.3 μm ratios, while the 6.2/11.3 μm ratio is 20% larger. Additionally, an error of perhaps 30% could be introduced by the uncertainty in the PAH molecular structure, i.e., the number of H atoms on a PAH and their distribution over groups of isolated, two adjacent and three adjacent atoms (§ 3.2.1).

It has been argued that the observed enhancement of the C—C modes at 6.2 and 7.7 μm with respect to the 11.3 μm C—H mode reflects almost complete dehydrogenation of the emitting PAHs (C/H > 100; Jourdain de Muizon et al. 1990a, b). However, as will be discussed in § 5.4, the observational

evidence suggests that the PAHs are not dehydrogenated by more than 50%. With less than 50% dehydrogenation, the amount of isolated H atoms on the carbon skeleton changes very little (§ 3.2.2), leaving the 7.7/11.3 μm intensity ratio essentially unchanged. In conclusion, we estimate that the uncertainties in the integrated cross sections per C—C or C—H bond adopted for the 6.2, 7.7, and 8.6 μm features of interstellar PAHs relative to the 11.3 μm band (Table 3) are of the order of 50%, 40%, and 50%, respectively.

5.4. *Dehydrogenation*

Originally, dehydrogenation was introduced to account for the presence of only C—H out-of-plane deformation modes corresponding to isolated Hs (Duley & Williams 1981). However, as subsequent observations have revealed the presence of the C—H deformation modes of doubly and/or triply adjacent C—H groups (Cohen et al. 1985; de Muizon et al. 1986; Roche et al. 1989; Witteborn et al. 1989), need for this drastic assumption has disappeared. Nevertheless, it has been suggested that the observed enhancement of the interstellar 7.7/11.3 μm band ratio with respect to laboratory spectra is due to strong dehydrogenation (~90%; Léger & d'Hendecourt 1987 and Jourdain de Muizon et al. 1990a). To investigate this possibility, a model spectrum was calculated using the laboratory-measured IR integrated cross sections (Table 3) and 95% dehydrogenated PAHs (Fig. 11). Although the spectrum reproduces the observed 7.7/11.3 μm ratio, a number of discrepancies are apparent with respect to the Orion Bar spectrum (Fig. 10) which arise from this high degree of dehydrogenation. First, the CH mode at 8.6 μm is much too weak. Second, the model does not reproduce the structure observed in the 11–14 μm C—H out-of-plane bending region. At this high degree of dehydrogenation, only isolated C—H groups survive, giving rise to the 11.3 μm band, while the two and three adjacent C—H groups responsible for the 12.7 μm feature have all but disappeared (§ 3.2.2). We conclude that dehydrogenation cannot be the cause of the enhancement of the 7.7 μm interstellar feature with respect to the 11.3 μm band.

Comparison of Figures 8*a*, 8*i*, 10, and 11 shows that the PAHs in the Orion Bar region can be at most ~50% dehydrogenated, provided the 12.7 μm feature originates from the out-of-plane bend of two adjacent H atoms (§ 5.3). At lower hydrogenation, the intensity of this mode relative to the 11.3 μm feature becomes much lower than observed, due to the low number of remaining groups of two adjacent H atoms (§ 3.2.2, Fig. 4). If the 12.7 μm feature is assigned to the out-of-plane bend of three adjacent H atoms, the maximum allowed dehydrogenation is even less. Additionally, comparing Figures 8*a*, 8*i*, 10, and 11 likewise suggests that the observed ratio of the 8.6 over the 7.7 μm feature excludes dehydrogenation in excess of about 50%. In fact, both the 12.7/11.3 μm and the 8.6/7.7 μm ratio are well reproduced by our 100% hydrogenated standard model. In this model the greater intensity of the 11.3 μm band relative to the 12.7 μm bands is in part a consequence of the intrinsic strengths of the respective modes. The integrated cross section per H atom for the isolated C—H group is measured to be twice that of two and three adjacent H atoms for PAHs in KBr pellets (Table 3). In addition, emission in the out-of-plane modes is dominated by very large PAHs (60–500 C atoms; see Fig. 9). Compact PAHs in this size range have similar numbers of isolated, two adjacent, and three adjacent C—H groups (§ 3.2.1) as opposed to the 20–40 C atom PAHs that have been studied in the laboratory. Here the number of isolated C—H groups is, in general, very small. We conclude that the emission spectrum toward the Orion Bar is consistent with fully hydrogenated PAHs, although a small degree of dehydrogenation (< 50%) cannot be excluded.

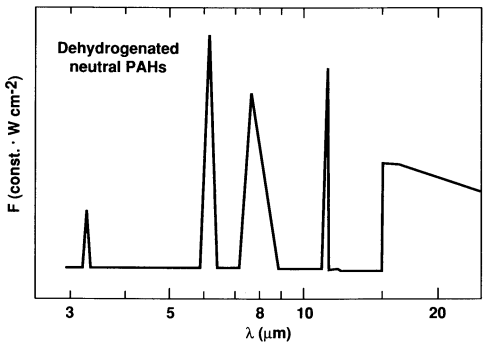

FIG. 11.—The model emission spectrum obtained using a fractional hydrogen coverage of $f_H = 0.05$ and the laboratory measured values of the integrated cross sections for the mid-IR modes (Table 3).

5.5. *The Interstellar* 3.4 *Micron Emission Feature and the Aromatic* C—H *Hot Band*

Emission in the 3 μm region from interstellar PAHs is generally characterized by a broad plateau with a number of superposed subfeatures along with the dominant 3.3 μm emission band (Geballe et al. 1985; Jourdain de Muizon et al. 1986; Jourdain de Muizon et al. 1990b; Nagata et al. 1988; Geballe et al. 1989; Lowe et al. 1991). It was suggested that the most prominent subfeature at 3.405 μm (henceforth the 3.4 μm feature) is due to the $v = 2$–1 "hot band" of the C—H stretching vibration, which, due to the large anharmonicity of the aromatic stretching mode, falls longward of the 3.3 μm $v = 1$–0 fundamental (Barker et al. 1987; Geballe et al. 1989). In the following we will investigate this possibility.

The ratio of the intensity of the $v = 2$–1 hot band to the $v = 1$–0 transition of the C—H stretching mode strongly increases with increasing vibrational energy of a PAH molecule (Barker et al. 1987). However, the ratio is bound to a maximum because, above a certain threshold energy E_{thr}, the molecule will lose its excess energy through C—H bond dissociation rather than through infrared fluorescence. To test the hot band model, this theoretical maximum is derived and compared to the observed 3.4/3.3 μm intensity ratios.

Table 6 lists E_{thr} for a number of aromatic molecules. These numbers were obtained using the RRKM theory to calculate the rate of C—H bond dissociation as a function of internal vibrational energy (Barker 1983; Tielens et al. 1987). Table 6 furthermore lists the maximum possible ratio of the $v = 2$–1 hot band to the $v = 1$–0 transition; i.e., at vibrational energy E_{thr}. Additionally, an "astronomical" maximum is listed, obtained by integrating the IR emission during relaxation from E_{thr} to energy 0. This maximum holds as long as multiphoton processes remain unimportant, which, for the small PAHs of Table 6, can be assumed in almost all interstellar environments (Table 5). It can be seen that the maximum possible intensity of the $v = 2$–1 hot band is equal to 0.17 times the $v = 1$–0 band intensity for benzene, and decreases with increasing molecular size.

The observed 3.4/3.3 μm intensity ratio is typically in the range 0.06–0.15. Our standard model results in a value of the $v = 2$–1 to $v = 1$–0 ratio of 0.08, within the observed range.

TABLE 6

THE C—H DISSOCIATION THRESHOLD ENERGY AND THE (MAXIMUM POSSIBLE) RATIO OF THE EMITTED FLUX IN THE $v = 2$–1 TO THE $v = 1$–0 TRANSITION OF THE C—H STRETCHING MODE FOR SOME SMALL PAHs

		$\frac{F(v=2\text{–}1)^b}{F(v=1\text{–}0)}$		
MOLECULE	E_{thr}[a] (cm^{-1})	Maximum	Astronomical Maximum	$T^* = 40{,}000$ K
Benzene	45,000	0.455	0.166	0.332
Naphthalene	58,000	0.333	0.126	0.202
Pyrene	78,000	0.280	0.117	0.114
Coronene	105,000	0.254	0.114	0.068

[a] Obtained with RRKM theory (Barker 1983).

[b] The maximum and astronomical maximum were obtained from the emission intensity ratio at E_{thr}, and by integrating the emission during relaxation from excitation energy E_{thr} to 0, respectively. The $T^* = 40{,}000$ K ratio was obtained by integrating the PAH emission after absorption of a photon over the stellar photon field, *not* taking into account cooling by dissociation of the C—H bond. In these calculations, the ratio of the $v = 2$–1 to the $v = 1$–0 emission intensity was obtained using exact densities of states.

However, the highest known ratio of 0.15, observed 20″ south of position 4 in the Orion Bar (Geballe et al. 1989), can, according to our calculations, be reproduced only by almost pure benzene emission. However, larger aromatic molecules up to $n_C \approx 80$ are likely to contribute to the emission in the 3 μm region as well (Fig. 9), and thus would lower the 3.4 to 3.3 μm ratio. It seems therefore unlikely that the hot band of the aromatic C—H stretching mode could be responsible for all of the 3.4 μm emission feature 20″ south of position 4 in the Orion Bar, and by inference elsewhere as well, unless the C—H band in the small PAHs which emit the C—H stretching fundamental and hot band are considerably more stable against fission than predicted by this model.

Another consequence of the hot band model that can be tested observationally involves variations in the overall relative band intensities which should accompany variations of the 3.4/3.3 μm ratio. An increase of the ratio is, in this model, due to increasing numbers of small PAHs ($n_C \lesssim 16$). Since such molecules contribute negligibly to the longer wavelength IR emission features (Fig. 9), a relative increase of the 3.3 μm band would then be expected. For example, in the Orion Bar region, the ratio of the intensity of the 3.4 μm band to that of the 3.3 μm feature increases with increasing distance from the exciting Trapezium stars. At position 4 the observed ratio equals 0.07, while 20″ south a ratio of 0.15 is found (Geballe et al. 1989). Table 6 lists the emission in the $v = 2$–1 hot band ratioed to the emission in the $v = 1$–0 transition for a number of small PAHs when exposed to a stellar field of temperature $T^* = 40{,}000$ K, the effective temperature of Θ^1 Ori C, the irradiating star in the Orion Bar. The $T^* = 40{,}000$ K column does not take into account the cooling by C—H bond dissociation which, as discussed above, likely occurs if the PAHs are sufficiently excited, and the listed values may therefore considerably overestimate the $v = 2$–1/1–0 ratio actually obtained. With these numbers the increase of the 3.3 μm feature relative to the longer wavelength bands was calculated. The minimum increase is obtained when assuming that an increased abundance of benzene is responsible for the increase in the 3.4/3.3 μm ratio. In this case, the intensity of the 3.3 μm band relative to the longer wavelength features should increase by 30% at the location 20″ south of position 4. For larger PAHs with a smaller $v = 2$–1 relative to $v = 1$–0 emission, the expected increase of the 3.3 μm band would be larger. For example, when the extra hot band emission is due to the addition of naphthalene molecules, an increase of the 3.3 μm feature by a factor of 2 is found. To take into account cooling by C—H bond dissociation at high excitation of the PAHs, we can alternatively use the $v = 2$–1/1–0 ratios listed in the "astronomical maximum" column in Table 6. This yields, if the extra 3.4 μm emission is caused by benzene, a predicted increase of the 3.3 μm feature 20″ south of position 4 equal to a factor of 3 relative to the longer wavelength emission features.

Thus, all other things being equal, the hot band model predicts an increase of the 3.3 μm feature relative to the longer wavelength features 20″ south of position 4 by at least 30%. Observations by Roche et al. (1989) of the 11.3 μm band and by Geballe et al. (1989) of the 3.3 μm feature toward position 4 and 20″ south indicate a nearly constant 3.3/11.3 μm ratio. However, since the intensities of the IR emission bands decrease strongly with increasing distance from the Trapezium stars (Geballe et al. 1989), small differences in the pointing of the telescope between these two data sets should lead to considerable error in the obtained 3.3/11.3 μm ratios. Nonetheless, variations of more than a factor of 2 can likely be excluded. Furthermore, local density fluctuations and inhomogeneities could alter the relative contributions from the large and small PAH populations. Thus, future observations in the Orion region are needed to further constrain the variations of the 3.3/11.3 μm intensity ratio and could serve as an important test of the hot band model.

In summary, both the observed absolute value of the 3.4/3.3 μm ratio and the spatial variation of the relative intensities of the IR emission bands in the Orion Bar region are only marginally consistent with the predictions from the hot band model. It seems therefore that there is another contributor to the 3.4 μm feature. Nonetheless, a separate hot band must be present in the emission of interstellar PAHs at some level. For example, our standard model with $\alpha = 3.5$ and $n_C(\text{min}) = 14$ yields a hot band to fundamental ratio of 0.079, while an alternative model with $\alpha = 4.5$, $n_C(\text{min}) = 20$, which gives a virtually identical overall emission spectrum, yields a ratio of 0.050. Thus, it is expected that detectable hot band emission be present near 3.4 μm. Perhaps the long-wavelength shoulder on the 3.4 μm feature near 3.415 μm observed toward NGC 7027 and Orion position 4 is this hot band (Barker et al. 1987), while the main feature originates from some other source (Lowe et al. 1991). Future observations of the variation of the intensity of this shoulder relative to the 3.3 μm feature and of the correlations between the 3.4 μm shoulder/3.3 μm intensity ratio, the 3.3/11.3 μm ratio, and the excitation radiation field are needed to further constrain the nature of these features.

5.6. *Aliphatic Sidegroups and "SPAHs"*

As an alternative to the hot band model, it has been suggested that the 3.4 μm feature is due to the asymmetric C—H stretching vibrations by aliphatic sidegroups on the PAH molecules (Duley & Williams 1981; de Muizon et al. 1986; Jourdain de Muizon et al. 1990b; Nagata et al. 1988). However, when measured in KBr and KI pellets, the $-CH_2-$ sidegroup band falls at 3.369 μm, well below the observed position at 3.405 μm. For $-CH_3$ sidegroups, on the other hand, this feature falls at 3.407 μm (d'Hendecourt & Léger 1987), but then a feature at 3.65 μm is expected to accompany the 3.405 μm band, and such a feature has not been found toward NGC

7027 (Sandford 1991). Sandford (1991) has also shown that there are several relative intensity discrepancies with the side-group model. Nevertheless, aliphatic sidegroups should not yet be excluded as the carrier of the 3.4 μm feature, since their vibrational frequencies on ionized or vibrationally excited free molecular PAHs are not known, and they might provide a better match to the interstellar data (de Muizon et al. 1986).

Another possibility is that some PAHs may have a number of hydrogen-saturated edge rings (de Groot 1991). These "superhydrogenated" PAHs ("SPAHs") would possess two C—H stretching bands, one due to the symmetric and the other to the asymmetric C—H stretching modes. If the molecules were fully (super-) hydrogenated (i.e., a cyclic aliphatic alkane such as cyclo-hexane), the bands would fall at about 2926 and 2853 cm^{-1} (3.418 and 3.505 μm), with the former more intense than the latter (Bellamy 1958; d'Hendecourt & Allamandola 1986). For PAHs which have H atoms added across a few double bonds as illustrated in Figure 12, the bands fall at about 2930 and 2820 cm^{-1} (3.41 and 3.55 μm), again with the former more intense (Sadtler Catalog of IR Spectra, 1966). These hydrogen atoms are quite labile. Having low bond dissociation energies, they are easily removed, restoring the rings' aromaticity (Stein & Brown 1991). Accepting this explanation for the moment—based on the observed 3.3/3.4 μm intensity ratio and assuming that aromatic and aliphatic CH band strengths apply (cf. Schutte et al. 1990)—implies that 1%–2% of interstellar PAH edge sites are superhydrogenated.

5.7. *The Size Distribution and Far-IR Emission*

The standard model reproduces the mid-IR emission spectrum toward Orion with a size distribution of steepness $\alpha = 3.5$ and $n_C(\text{min}) = 14$. However, since changing the minimum PAH size and steepness (α) influence the emission spectrum in a similar fashion (cf. Figs. 8*a*–8*d*), this fit is certainly not unique. In fact, if exclusively considering the mid-IR emission, a good fit could be obtained with a "size distribution" containing a single PAH of about 40 C atoms (Figs. 9 and 10; see also § 1 and references therein). Additional uncertainty in the size distribution is introduced by a possible difference between the integrated cross section of the 3.3 μm C—H stretching mode for laboratory measured and interstellar PAHs (cf. DeFrees et al. 1993).

The ratio of the mid- to far-IR emission gives a better constraint on the size distribution of the PAHs, since it is only little influenced by the value of $n_C(\text{min})$, while the effect of α is quite large (cf. Figs. 8*a*–8*d*). Unfortunately, the uncertainty in PAH far-IR absorption properties limits the accuracy to which α can be determined (Figs. 8*a*, 8*g*, and 8*h*). The ratio of the *IRAS* 12 and 25 μm photometric fluxes observed in the diffuse medium varies between 0.7 and 1.5, with an average of ~ 1.0 (Chlewicki & Laureys 1988). A model with the standard parameters but $T^* = 10{,}000$ K (the approximate temperature of the interstellar radiation field; Spitzer 1978) yields a ratio of 0.79. Apparently, the standard MRN-type size distribution for PAHs with $14 \leq n_C \lesssim 10^5$ reproduces the far-IR broad-band emission reasonably well. This result supports the assumption of the presence of a continuous size distribution of PAHs, since such models can simultaneously match the spectral distribution in the mid-IR as well as the relative intensities of the mid- and far-IR emission in the *IRAS* broad bands (see also Puget et al. 1985; Désert et al. 1990). Models with $\alpha = 2.5$ and 4.5 give 12 to 25 μm band ratios of 0.36 and 1.65, respectively (Table 4), outside the range of observed values. However, due to the uncertainty in the far-IR cross sections and possible contributions to the 25 μm emission by particles of size 10^3–10^5 atoms other than PAHs, size distributions with steepness somewhere in the range should not be excluded.

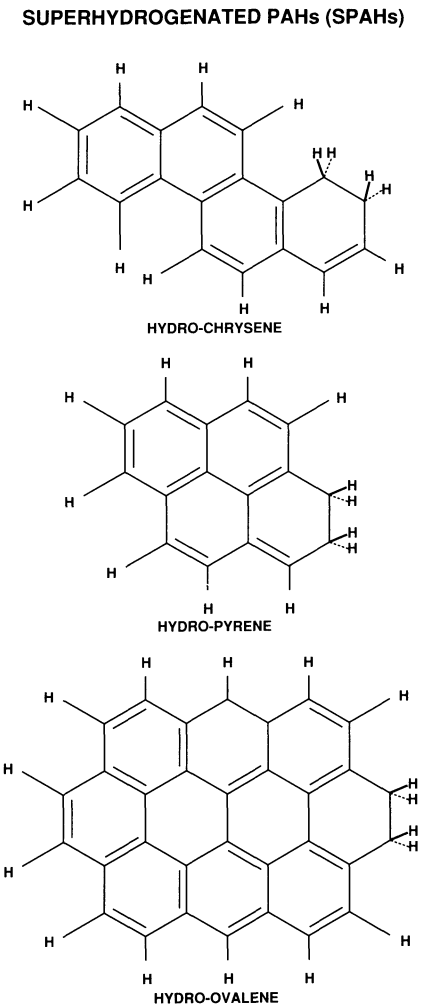

FIG. 12.—Some examples of "superhydrogenated" PAHs (SPAHs)

As described in § 3.2.7, Désert et al. (1990) fitted the mid- and far-IR emission (up to 50 μm) using two populations of grains (PAHs and VSGs). The mid-IR emission resulting from this model is quite similar to that of our standard model. The steepness of the PAH size distribution is much smaller than that of our standard model while the minimum PAH size is somewhat larger, resulting in more emission in the 6.2, 7.7, and 11.3 μm features relative to the 3.3 μm feature from PAHs smaller than $n_C = 150$. This difference is compensated for by the lack of PAHs with more than 150 C atoms, which, in our model, strongly contribute to the 6.2, 7.7, and 11.3 μm bands (Fig. 9). Likewise, the relative far- and mid-IR emission is quite similar for the Désert et al. model and our standard model. Here, the various differences between our two approaches offset one another. On the one hand, the number of particles with $n_C > 10^3$ relative to PAHs with less than 150 C atoms is considerably smaller in the Désert et al. model. This decreases the far-IR relative to mid-IR emission. However, this is offset by the dearth of particles containing between 150 and 10^3 C atoms in the Désert et al. model. These contribute a large

fraction of the mid-IR emission in our model (Fig. 9). As this comparison illustrates, the details of the size distribution are not well constrained, and presently no model can "claim" to be unique. Further tests will be provided by theoretical and observational studies of regions with varying incident UV fluxes.

6. CONCLUSIONS

We have synthesized mid-IR (2.8–13 μm) emission spectra from four well-studied PAH emission sources: HD 44179, NGC 7027, BD 30°3639, and position 4 in the Orion Bar. An inverse correlation of the observed feature-to-continuum ratio with the UV/visual flux level in these sources suggested that the features originate in small species ($\lesssim 10^3$ C atoms), while the continuum is dominated by larger particles which are excited by multiphoton processes.

We have modeled the spectrum of the family of IR emission bands observed toward the Orion Bar region by calculating the emission from a size distribution of interstellar PAHs. It was found that the various emission bands in the mid-IR (2.5–15 μm), as well as the far-IR continuum emission, are dominated by PAHs of distinctly different sizes, from $\lesssim$80 C atoms for the 3.3 μm feature, to 10^2–10^5 C atoms for the PAHs emitting in the 25 μm *IRAS* band. The observed relative intensities of the various mid-IR bands and the far-IR continuum are therefore sensitive indicators of the size distribution of interstellar PAHs.

A number of properties of interstellar PAHs have been derived. The observed intensities of the 8.6 μm C—H in-plane bending and of the 12.7 μm feature of the C—H out-of-plane bending mode of two or of three adjacent H atoms indicate that interstellar PAHs are more than 50% hydrogenated and are indeed quite consistent with 100% hydrogenation. This confirms the results of earlier calculations which showed that for all but the smallest species ($n_C \lesssim 24$), the C—H bonds of interstellar PAHs should not be susceptible to photodissociation. We therefore interpret the observed enhancement of the 6.2 and 7.7 μm C—C stretching modes and the 8.6 μm C—H in-plane bending mode relative to laboratory PAHs to an increase of the intrinsic strengths of these modes by factors of 2–6 rather than to dehydrogenation. Such an enhancement could perhaps be related to interstellar PAHs being singly ionized. DeFrees et al. (1993) calculated the effects of ionization on the IR properties for a number of small PAHs and found large enhancements of the intensities of the C—C stretching features. Laboratory measurements on ionized PAHs now underway at Ames (Hudgins, Sandford, & Allamandola 1993) and the University of Florida (by Vala, Szczepanski, and coworkers) support this prediction. Alternatively, by virtue of their size, the larger PAHs which contribute to these longer mid-IR bands will be intrinsically more stable against photodestruction than the smaller members of the PAH family, and thus less symmetric species should be present. As symmetry is lowered, more C—C modes become IR active. Thus it is plausible that some of the C—C mode enhancement is due to contributions from larger, less symmetric PAHs.

In our model all particles consist of a single, flat aromatic structure. Part of the larger particle family with perhaps $n_C \geq 100$ could possibly be amorphous carbon–like (i.e., clustered aromatic structures connected by aliphatic chains). The main effect of including such a population of particles while otherwise keeping the size distribution constant—i.e., the same number of particles containing a certain number of C atoms stays the same—would be a rise in the relative number of aromatic H to aromatic C atoms. For example, if the particles above 100 C atoms consist of clusters of smaller PAHs, this could raise the relative amount of H atoms in these particles by a factor of 2–4. To compensate for the resulting increase in the 3.3, 8.6, 11.3, 12.7, and 13.3 μm features, the enhancement of the intrinsic strengths of the 6.2 and 7.7 μm features relative to laboratory measurements would then have to be larger by factors of 2 and 6, respectively.

The suggestion that the subfeature at 3.4 μm is due to the $v = 2$–1 hot band of the aromatic C—H stretching mode was also tested. The largest observed intensity of the feature relative to the 3.3 μm band (as well as the apparent lack of spatial variation of the 3.3/11.3 μm ratio accompanying the spatial variation of the 3.4/3.3 μm ratio) in the Orion Bar region seems only marginally consistent with the predictions of the hot band model. Possibly a weak shoulder at 3.415 μm observed toward a number of sources rather than the main 3.4 μm feature itself should be assigned to the hot band of the aromatic C—H stretching mode. An alternative assignment of the 3.4 μm band may involve "superhydrogenated" PAHs (SPAHs), i.e., PAHs for which some of the peripheral carbon atoms of the edge rings are bonded to two H atoms. The positions of the symmetric and asymmetric C—H stretching bands of such groups falls quite close to the frequencies of the interstellar features. Such an identification would imply that 1%–2% of the peripheral bonding sites of the PAHs toward the Orion Bar are connected to two H atoms.

The standard model reproduces, reasonably well, the observed ratio of the *IRAS* 12 μm and 25 μm photometric fluxes in the diffuse medium using an MRN-type power-law size distribution and the far-IR properties measured in the laboratory for an ensemble of small PAHs. The success of this standard model in simultaneously fitting the observed mid-IR spectrum and the relative far- to mid-IR emission level strongly supports our assumption of the presence of a continuous size distribution of PAHs or PAH clusters containing between 10 and 10^5 C atoms.

Future high-sensitivity, single-aperture observations of the entire emission spectrum from 3 μm to far-IR wavelengths as will likely be obtained by the *Infrared Space Observatory* (*ISO*) and *Space Infrared Telescope Facility* (*SIRTF*), together with theoretical modeling of the type presented in this paper could answer a number of important questions. First, the nature of the 3.405 μm subfeature and its 3.415 μm shoulder could be further clarified by studying the intensity variations of these bands and their correlation with the relative intensities of the other IR emission features. The discovery of the hot band of the aromatic C—H stretching mode would place a very important constraint on the sizes of the smallest molecules in the PAH size distribution (§ 5.5). Furthermore, the possibility that the 3.4 μm feature originates in interstellar SPAHs could be tested by searching for the $-CH_2-$ deformation mode at 6.8 μm. Second, source-to-source variations of the relative intensities of the mid-IR features and far-IR continuum could reveal variations in the size distribution of interstellar PAHs. Third, detection of resolved emission bands in the far-IR ($\lambda \geq 15$ μm) may lead to a determination of the abundances of individual PAHs, since the positions of the vibrational modes in this region are highly characteristic of specific molecules (§ 3.2.4.2). Fourth, moderate-resolution observations beyond 13 μm will determine the existence of additional C—H out-of-plane bending features besides the 11.3 and 12.7 μm bands. The relative intensities of the various out-of-plane features will give important information of the molecular structure of interstellar

PAHs as well as on their degree of hydrogenation (§§ 3.2.1, 3.2.2, and 5.4). Finally, studying the properties of "young" PAHs in planetary nebulae and those of "old" PAHs in reflection nebulae and cirrus clouds could lead to a better understanding of the evolution of PAHs in the interstellar medium.

It is a pleasure to acknowledge John Barker for his invaluable support and many useful suggestions as well as for making his numerical code for exact density of state calculations available to us. This research was supported by NASA grant 188-41-57 from the Infrared/Radio Astrophysics Branch.

REFERENCES

Allamandola, L. J., Bregman, J. D., Sandford, S. A., Tielens, A. G. G. M., Witteborn, F. C., Wooden, D. H., & Rank, D. 1989, ApJ, 345, L59
Allamandola, L. J., Tielens, A. G. G. M., & Barker, J. R. 1985, ApJ, 290, L25
———. 1989, ApJS, 71, 733 (ATB)
Arens, J. F., Lamb, G. M., Peck, M. C., Moseley, H., Hoffmann, W. F., Tresch-Fienberg, R., & Fazio, G. G. 1984, ApJ, 279, 685
Barker, J. R. 1983, Chem Phys., 77, 301
Barker, J. R., Allamandola, L. J., & Tielens, A. G. G. M. 1987, ApJ, 315, L61
Barker, J. R., & Cherchneff, I. 1989, in IAU Symp. 135, Interstellar Dust, ed. L. J. Allamandola & A. G. G. M. Tielens (Dordrecht: Kluwer), 197
Becklin, E. E., Beckwith, S., Gatley, I., Matthews, K., Neugebauer, G., Sarazin, C., & Werner, M. W. 1976, ApJ, 207, 770
Bellamy, L. J. 1970, The Infrared Spectra of Complex Molecules (New York: John Wiley & Sons)
Bree, A., Kydd, R. A., Misra, T. N., & Vilkos, V. V. B. 1971, Spectrochim. Acta, 27A, 2315
Bregman, J. D., Allamandola, L. J., Tielens, A. G. G. M., Geballe, T. R., & Witteborn, F. C. 1989, ApJ, 344, 791
Buss, R. H., Cohen, M., Tielens, A. G. G. M., Werner, M. W., Bregman, J. D., Witteborn, F. C., & Sandford, S. A. 1990, ApJ, 365, L23
Bussoletti, E., Colangeli, L., Borghesi, A., & Orofino, V. 1987, A&AS, 70, 257
Chlewicki, G., & Laureys, R. J. 1988, A&A, 207, L11
Clar, E. 1952, The Aromatic Sextet (London: Wiley)
Cohen, M., Allamandola, L. J., Tielens, A. G. G. M., Bregman, J., Simpson, J. P., Witteborn, F. C., Wooden, D., & Rank, D. 1986, ApJ, 302, 737
Cohen, M., Tielens, A. G. G. M., & Allamandola, L. J. 1985, ApJ, 299, L93
Cohen, M., Tielens, A. G. G. M., Bregman, J., Witteborn, F. C., Rank, D. M., Allamandola, L. J., Wooden, D. H., & de Muizon, M. 1989, ApJ, 341, 246
Cyvin, S. J., & Klaeboe, P. 1988, private communication
DeFrees, D. J., Miller, M. D., Talbi, D., Pauzat, F., & Ellinger, Y. 1993, ApJ, 408, 530
de Groot, M. S. 1990, private communication
de Muizon, M., Geballe, T. R., d'Hendecourt, L. B., & Baas, F. 1986, ApJ, 306, L105
Désert, F. X., Boulanger, F., & Puget, J. L. 1990, A&A, 237, 215
d'Hendecourt, L. B., & Allamandola, L. J. 1986, A&AS, 64, 453
d'Hendecourt, L. B., & Léger, A. 1987, in Planetary and Protoplanetary Nebulae: From IRAS to ISO, ed. A. Preite Martinez (Dordrecht: Reidel), 203
d'Hendecourt, L. B., Léger, A., Boissel, P., & Désert, F. X. 1989, in IAU Symp. 135, Interstellar Dust, ed. L. J. Allamandola & A. G. G. M. Tielens (Dordrecht: Kluwer), 207
Donn, B. 1988, private communication
Donn, B. D., Allen, J. E., & Khanna, R. K. 1989, in IAU Symp. 135, Interstellar Dust, ed. L. J. Allamandola & A. G. G. M. Tielens (Dordrecht: Kluwer), 181
Draine, B. T. 1984, ApJ, 277, L71
———. 1985, ApJS, 57, 587
Draine, B. T., & Anderson, N. 1985, ApJ, 292, 494
Draine, B. T., & Lee, H. M. 1984, ApJ, 285, 89
Duley, W. W., & Williams, D. A. 1981, MNRAS, 196, 269
Dwek, E. 1986, ApJ, 302, 363
Geballe, T. R., Lacy, J. H., Persson, S. E., McGregor, P. J., & Soifer, B. T. 1985, ApJ, 292, 500
Geballe, T. R., Tielens, A. G. G. M., Allamandola, L. J., Moorhouse, A., & Brand, P. W. J. L. 1989, ApJ, 341, 278
Gutfreund, H., & Little, W. A. 1969, J. Chem. Phys., 50, 4468
Hora, J. L., Deutsch, L. K., Hoffmann, W. F., & Fazio, G. G. 1990, ApJ, 353, 549
Hudgins, D. M., Sandford, S. A., & Allamandola, L. J. 1993, J. Phys. Chem., submitted
Jaffe, H. H., & Orchin, M. 1962, Theory and Applications of Ultraviolet Spectroscopy (New York: J. Wiley & Sons)
Jourdain de Muizon, M., d'Hendecourt, L. B., & Geballe, T. R. 1990a, A&A, 227, 526
———. 1990b, A&A, 235, 367
Jourdain de Muizon, M., d'Hendecourt, L. B., Geballe, T. R., & Baas, F. 1986, ApJ, 306, L105
Léger, A., Boissel, P., Desert, F. X., & d'Hendecourt, L. 1989a, A&A, 213, 351
Léger, A., & d'Hendecourt, L. 1987, in Polycyclic Aromatic Hydrocarbons and Astrophysics, ed. A Léger, L. d'Hendecourt, & N. Boccara (Dordrecht: Reidel), 223
Léger, A., d'Hendecourt, L. B., & Défourneau, D. 1989b, A&A, 216, 148
Léger, A., & Puget, J. L. 1984, A&A, 137, L5
Lowe, R. P., Moorhead, J. M., Wehlau, W. H., & Maillard, J.-P. 1991, ApJ, 368, 195
Mathis, J. S., Rumpl, W., & Nordsieck, K. H. 1977, ApJ, 217, 425
McClellan, A. L., & Pimentel, G. C. 1955, J. Chem. Phys., 23(2), 245
Merrill, K. M., Soifer, B. T., & Russell, R. W. 1975, ApJ, 200, L37
Nagata, T., Tokunaga, A. T., Sellgren, K., Smith, R. G., Onaka, T., Nakada, Y., & Sakata, A. 1988, ApJ, 326, 157
Phillips, M. M., Aitken, D. K., & Roche, P. F. 1984, MNRAS, 207, 25
Platt, J. R. 1956, ApJ, 123, 486
Pottash, S. R. 1984, Planetary Nebulae (Dordrecht: Reidel)
Puget, J. L., & Leger, A. 1989, ARA&A, 27, 161
Puget, J. L., Leger, A., & Boulanger, F. 1985, A&A, 142, L19
Robertson, J. 1986, Adv. Phys., 35(4), 317
Roche, P. F., & Aitken, D. K. 1985, MNRAS, 213, 789
Roche, P. F., Aitken, D. K., & Smith, C. H. 1989, MNRAS, 236, 485
Russell, R. W., Soifer, B. T., & Merrill, K. M. 1977a, ApJ, 213, 66
Russell, R. W., Soifer, B. T., & Willner, S. P. 1977b, ApJ, 217, L149
———. 1978, ApJ, 220, 568
Sandford, S. A. 1991, ApJ, 376, 599
Schutte, W. A., Tielens, A. G. G. M., Allamandola, L. J., Cohen, M., & Wooden, D. H. 1990, ApJ, 360, 577
Sellgren, K. 1984, ApJ, 277, 623
Spitzer, L. 1978, Physical Processes in the Interstellar Medium (New York: Wiley)
Sadtler Atlas of Infrared Spectra. 1966, Sadtler Research Laboratories, Pennsylvania
Stein, S. E., & Brown, R. L. 1991, J. Am. Chem. Soc., 113, 787
Stein, S. E., Golden, D. M., & Benson, S. W. 1977, J. Phys. Chem., 81, 314
Stein, S. E., & Rabinovitch, B. S. 1973, J. Chem. Phys., 58(6), 2438
Tanabé, T., Nakada, Y., Kamijo, F., & Sakata, A. 1983, PASJ, 35, 397
Tielens, A. G. G. M. 1989, in Submillimetre Wave Astronomy, ed. E. D. Watt & D. S. Webster (Dordrecht: Kluwer), 13
Tielens, A. G. G. M., Allamandola, L. J., Barker, J. R., & Cohen, M. 1987, in Polycyclic Aromatic Hydrocarbons and Astrophysics, ed. A. Léger, L. d'Hendecourt, & N. Boccara (Dordrecht: Reidel), 273
Touloukian, Y. S., & Buyco, E. H. 1970, Thermophysical Properties of Matter, Vol. 5 (New York: Plenum)
van der Zwet, G. P., & Allamandola, L. J. 1985, A&A, 146, 76
Wdowiak, T. 1989, private communication
Whitten, G. Z., & Rabinovitch, B. S. 1963, J. Chem. Phys., 38(10), 2466
Witteborn, F. C., Sandford, S. A., Bregman, J. D., Allamandola, L. J., Cohen, M., Wooden, D. H., & Graps, A. L. 1989, ApJ, 341, 270